Empirical strong-line oxygen abundance calibrations from galaxies with electron-temperature measurements

S. Y. Yin, Y. C. Liang, F. Hammer, J. Brinchmann, B. Zhang, L. C. Deng, H. Flores

A&A 462, 535–546 (2007)
DOI: 10.1051/0004-6361:20065798

Astronomy & Astrophysics

Empirical strong-line oxygen abundance calibrations from galaxies with electron-temperature measurements⋆

S. Y. Yin[1,3], Y. C. Liang[1,2], F. Hammer[2], J. Brinchmann[4], B. Zhang[1,3], L. C. Deng[1], and H. Flores[2]

[1] National Astronomical Observatories, Chinese Academy of Sciences, 20A Datun Road, Chaoyang District, Beijing 100012, PR China
e-mail: [syyin;ycliang]@bao.ac.cn
[2] GEPI, Observatoire de Paris-Meudon, 92195 Meudon, France
[3] Department of Physicals, Hebei Normal University, Shijiazhuang 050016, PR China
[4] CAUP, Rua das Estrelas S/N, 4150-752 Porto, Portugal

Received 10 June 2006 / Accepted 27 September 2006

ABSTRACT

Aims. Our aims are to estimate the validity of empirical methods, such as R_{23}, $R_{23} - P$, log([N II]/Hα) (N2), log[([O III]/Hβ)/([N II]/Hα)] (O3N2), and log([S II]/Hα) (S2), and to re-derive (or add) the calibrations of R_{23}, N2, O3N2, and S2 indices for oxygen abundances on the basis of a large sample of galaxies with T_e-based abundances.
Methods. We determined the gas-phase oxygen abundance for a sample of 695 galaxies and H II regions with reliable detections of [O III]4363, using the reliable and direct temperature-sensitive (T_e) method of measuring metallicity. We selected 531 star-forming galaxies from the SDSS-DR4 database with strong emission lines, including [O III]4363 detected at a signal-to-noise ratio higher than 5σ, as well as 164 galaxies and H II regions from the literature with T_e measurements. The O/H abundances were derived from a two-zone model for the temperature structure, assuming a relationship between high ionization and low ionization species.
Results. We compare our $(O/H)_{T_e}$ measurements of the SDSS sample with the abundances obtained by the MPA/JHU group who used multiple strong emission lines and Bayesian techniques (Tremonti et al. 2004). For roughly half of the sample the Bayesian abundances are overestimated ~0.34 dex, possibly due to the treatment of nitrogen enrichment in the models they used. The R_{23} and $R_{23} - P$ methods systematically overestimate the O/H abundance by a factor of ~0.20 dex and ~0.06 dex, respectively. The N2 index, rather than the O3N2 index, provides more consistent O/H abundances with the T_e-method, but with some scatter. The relations of N2, O3N2, and S2 with log(O/H) are consistent with the photoionization model calculations of Kewley & Doptita (2002), but R_{23} does not match well. We derive analytical calibrations for O/H from R_{23}, N2, O3N2, and S2 indices on the basis of this large sample, including the excitation parameter P as an additional parameter in the N2 calibration. These empirical calibrations are free of the systematic problems inherent in abundance calibrations based on photoionization models.
Conclusions. We conclude that the N2, O3N2, and S2 indices are useful indicators for calibrating metallicities of galaxies with 12 + log(O/H) < 8.5 and that the R_{23} index works well for the metal-poor galaxies with 12+log(O/H) < 7.9. For the intermediate metallicity range (7.9 < 12 + log(O/H) < 8.4), the R_{23} and $R_{23} - P$ methods are unreliable for characterizing the O/H abundances,

Key words. galaxies: abundances – galaxies: evolution – galaxies: ISM – galaxies: spiral – galaxies: starburst – galaxies: stellar content

1. Introduction

The chemical properties of stars and gas within a galaxy provide both a fossil record of its star formation history and information on its present evolutionary status. It is therefore desirable to extract as much accurate information as possible from observations of galaxies. In particular, it is important that different methods of extracting information provide this without systematic offsets or, at the very least, that these systematic offsets are understood well. Accurate abundance measurements for the ionized gas in galaxies require the determination of the electron temperature (T_e) in this gas, which is usually obtained from the ratio of auroral to nebular line intensities, such as [O III]$\lambda\lambda$4959, 5007/[O III]λ4363. This is generally known as the "direct T_e-method" because the electron temperature is directly inferred from observed line ratios. It is well known that this procedure is difficult to carry out for metal-rich galaxies since, as the metallicity increases, the electron temperature decreases (as the cooling is via metal lines), and the auroral lines eventually become too faint to measure. Instead, the most common method used for estimating oxygen abundance of metal-rich galaxies (12+log(O/H) ≥ 8.5) uses the R_{23} (=([O II]λ3727+[O III]$\lambda\lambda$4959,5007)/Hβ) parameter, which is the ratio of the flux in the strong optical oxygen lines to that of Hβ (Pagel et al. 1979; Tremonti et al. 2004 and the references therein). The R_{23} indicator can also be used for metal-poor galaxies (12+log(O/H) < 8.5) (Skillman et al. 1989; Kobulnicky et al. 1999; McGaugh 1991; Pilyugin 2000; Edmunds & Pagel 1984).

Several researchers have found, however, that R_{23}-derived abundances are inconsistent with the T_e-derived ones, showing a systematic offset. For example, Kennicutt et al. (2003) found that R_{23} overestimates the actual log(O/H) abundance by a factor of 0.2–0.5 dex using a sample of 20 H II regions in M 101 with high-S/N spectra. Some other research found similar results, for example, Bresolin et al. (2004, 2005), Garnett et al. (2004a,b), Pilyugin (2006), Shi et al. (2005, 2006). A much larger dataset

⋆ Table 1 is only available in electronic form at http://www.aanda.org

can help to understand this effect better, as well extending it to galaxies.

To estimate abundances of galaxies, when T_e and R_{23} cannot be used, some other metallicity-sensitive "strong-line" ratios are very useful, for example, [N II]λ6583/Hα, [O III]λ5007/[N II]λ6583, [N II]λ6583/[O II]λ3727, [N II]λ6583/[S II]$\lambda\lambda$6717,6731, [S II]$\lambda\lambda$6717,6731/Hα, and [O III]$\lambda\lambda$4959,5007/Hβ (Liang et al. 2006; Nagao et al. 2006; Pérez-Montero & Díaz 2005; Pettini & Pagel 2004, hereafter PP04; Denicoló et al. 2002, hereafter D02; Kewley & Dopita 2002, hereafter KD02). Even when R_{23} is available, some of these line-ratios are useful for overcoming the well-known problem that the R_{23} vs. 12 + logO/H relation is double-valued, and further information is required to break this degeneracy. Alternative methods of breaking the degeneracy when a well-established luminosity-metallicity relation exists or when the likelihood of each branch can be calculated, which is discussed by Lamareille et al. (2006).

Strong-line abundance indicators are typically calibrated in one of two ways: (1) using the samples of galaxies with direct (T_e-based) abundances (e.g. PP04; Pagel et al. 1979, etc.) or (2) using photoionization models (e.g. McGaugh 1991; Tremonti et al. 2004, etc.). Since the T_e-method is generally thought to be the most accurate method for metallicity estimation, we will take oxygen abundances derived using this method as our baseline. We selected a large sample of 531 galaxies from the Fourth Data Release of the Sloan Digital Sky Survey database (SDSS-DR4) with their [O III]λ4363 emission line detected at an S/N higher than 5σ and 164 associated galaxies and H II regions from the literature. We compared their T_e-based O/H abundances with the Bayesian estimates provided by the MPA/JHU group (shown as $\log(O/H)_{Bay}$), which were obtained by fitting multi-emission lines using the photoionization models of Charlot et al. (2006), and with those derived from some strong-line ratios given in previous studies, including R_{23}, P, N2, O3N2 methods, etc. (Kobulnicky et al. 1999; Pilyugin 2001; PP04). We also compared the observational results with the photoionization model results of KD02 for the relations of O/H vs. R_{23}, N2, O3N2 and S2 indices.

Our particular concern in this study is the abundance calibrations of strong-line ratios on the basis of their T_e-based metallicities. When we compare the observational relations of O/H vs. strong-line ratios with the photoionization model results of KD02, we find that only the N2, O3N2, S2 indices are useful for estimating abundances for galaxies with low metallicity, $12+\log(O/H)_{T_e} < 8.5$, while other line ratios, such as [N II]/[O II], [N II]/[S II], and [O III]/Hβ are not good indicators for this metallicity range due to their insensitivity to metallicities there, except in the extremely metal-poor environments (e.g. 12+log(O/H) < 7.5 or 7.0) (Stasińska 2002; KD02). The value of R_{23} is a useful indicator of metallicity for the low metallicity region with 12+log(O/H) < 7.9. Thus, we will only calibrate the relationships of the R_{23}, N2, O3N2, and S2 indices to O/H abundances from the observational data in this study. Moreover, for the N2 index, we follow Pilyugin (2000, 2001a,b) to add the excitation parameter P (=[O III]/([O II]+[O III])) to separate the sample galaxies into three sub-samples in the calibrations. These calibrations can be the extension of the metal-rich region studied by Liang et al. (2006) to the low-metallicity region.

This paper is organized as follows. The sample selection criteria are described in Sect. 2. The determinations of the oxygen abundances from T_e are presented in Sect. 3. In Sect. 4, we present the comparisons between the $(O/H)_{T_e}$ and the $(O/H)_{Bay}$, as well as those abundances derived from other strong-line relations. Section 5 shows the comparison of the observational data with the photoionization models of KD02. In Sect. 6, we rederive analytical calibrations between O/H and R_{23}, N2, O3N2, S2 indices, as well the two-parameter calibrations for the N2 index with the P-parameter included. The conclusions are given in Sect. 7.

2. Observational data

We selected 531 galaxies from the SDSS-DR4 (Adelman-McCarthy et al. 2006) and gathered 164 low-metallicity H II regions and galaxies from the literature in this study.

2.1. The SDSS-DR4 data

The SDSS-DR4 provides spectra in the wavelength range ~3800–9200 Å for >500 000 galaxies over 4783 square degrees[1]. The MPA-JHU collaboration has in addition measured emission-line fluxes and some derived physical parameters for a sample of 520 082 unique galaxies at the MPA SDSS website[2]. Therefore, we call the working sample selected in this study as the "MPA/JHU sample" hereafter. We have selected the "star-forming galaxies" with metallicity measurements and identified them following the selection criteria of the traditional line diagnostic diagram [N II]/Hα vs. [O III]/Hβ (Baldwin et al. 1981; Veilleux & Osterbrock 1987; Kewley et al. 2001; Kauffmann et al. 2003). The fluxes of emission-lines were measured from the stellar-feature-subtracted spectra with the spectral population synthesis code of Bruzual & Charlot (2003; Brinchmann et al. 2004; Tremonti et al. 2004).

We selected the galaxies with redshifts $0.03 < z < 0.25$ to make certain to cover from [O II] to Hα and [S II] emission lines. Tremonti et al. (2004) also discuss the weak effect of aperture on estimated metallicities of the sample galaxies with $0.03 < z < 0.25$, and this was discussed further by Kewley et al. (2005), but for the present study the aperture effects are unimportant.

In this study, we used the T_e-method to derive O/H abundances of the sample galaxies (see Sect. 3 for details); therefore, we selected the samples with the [O III]λ4363 emission-line detected where the *S/N* is higher than 5σ. To be consistent with Liang et al. (2006) and Tremonti et al. (2004), we also considered the objects with measured fluxes of [O II]$\lambda\lambda$3726,3729, [O III]λ5007, Hβ, Hα, [N II]λ6583, [S II]$\lambda\lambda$6717, 6731 emission lines, and the *S/N* of Hβ, Hα, [N II], [S II] are larger than 5σ. The final sample consists of 531 galaxies. These have fluxes in [O III]λ4363 greater than 5.3×10^{-17} erg s^{-1} cm^{-2}, with a mean value of 21.27×10^{-17} erg s^{-1} cm^{-2}.

The fluxes of the emission lines are corrected for dust extinction, which are estimated using the Balmer-line ratio Hα/Hβ, and assuming case B recombination, with a density of 100 cm^{-3} and a temperature of 10^4 K, and the intrinsic ratio of Hα/Hβ is 2.86 (Osterbrock 1989), with the relation of $(\frac{I_{H\alpha}}{I_{H\beta}})_{obs} = (\frac{I_{H\alpha0}}{I_{H\beta0}})_{intr} 10^{-c(f(H\alpha)-f(H\beta))}$. Using the average interstellar extinction law given by Osterbrock(1989), we have $f(H\alpha) - f(H\beta) = -0.37$. For the 56 data points with $c < 0$, we assume they have $c = 0$ since their intrinsic Hα/Hβ may be lower than 2.86 if their electron temperature is high (Osterbrock 1989, p. 80).

Nearly all previous empirical oxygen abundance calibrations were derived from individual H II regions since it is much easier

[1] http://www.sdss.org/dr4/

[2] http://www.mpa-garching.mpg.de/SDSS/

to detect [O III]4363 that way. In contrast, the SDSS data samples the inner few kpc of most galaxies. One question is whether the global spectrum from a mixture of different H II regions will yield meaningful average abundances of the galaxies or not. Kobulnicky et al. (1999), Moustakas & Kennicutt (2006), and Pilyugin et al. (2004) all conclude that the spatially unresolved emission-line spectra can reliably indicate the chemical properties of distant star-forming galaxies. However, as Kobulnicky et al. (1999) mention, the standard nebular chemical abundance measurement methods may be subject to small systematic errors when the observed volume includes a mixture of gas with diverse temperatures, ionization parameters, and metallicities. For the low-mass, metal-poor galaxies, such as those we are studying in this work, standard chemical analyses using global spectra will overestimate the electron temperatures T_e due to the non-uniform T_e and large variations in the ionization parameter since the global spectra are biased toward the objects with stronger emission lines. As a result, the oxygen abundances derived from T_e will be underestimated, i.e. about <0.1 dex in log(O/H) (for more massive metal-rich galaxies like local spiral galaxies, there is about ±0.2 dex discrepancy). However, since this bias is small, and not well-constrained for our dataset, we do not attempt to correct for it.

2.2. The metal-poor galaxies from the literature

In addition to the MPA/JHU samples, we also collected 164 low-metallicity samples including some blue compact galaxies (BCDs) and H II regions from the literature, which were taken from Izotov et al. (1994, 1996, 1997a,b, 1999, 2001a,b, 2004), Izotov & Thuan (1998a,b, 1999, 2004), van Zee (2000), Kniazev et al. (2000), Vilchez et al. (2003), Guseva et al. (2003a,b,c), Melbourne et al. (2004), and Lee et al. (2004). There are 110 H II regions and 54 galaxies in this sample.

We re-estimated their O/H abundances by using the electronic temperatures method given in Sect. 3. Their metallicities are 7.1 < 12+log(O/H) < 8.4, more metal-poor than the SDSS galaxies generally. To check if there is systematic difference between our estimates and the values given in the previous studies, we compared their T_e-based oxygen abundances obtained by us with those T_e-based given in the original reference in Fig. 1, which shows that they are very consistent, and the very slight difference may come from different atomic data.

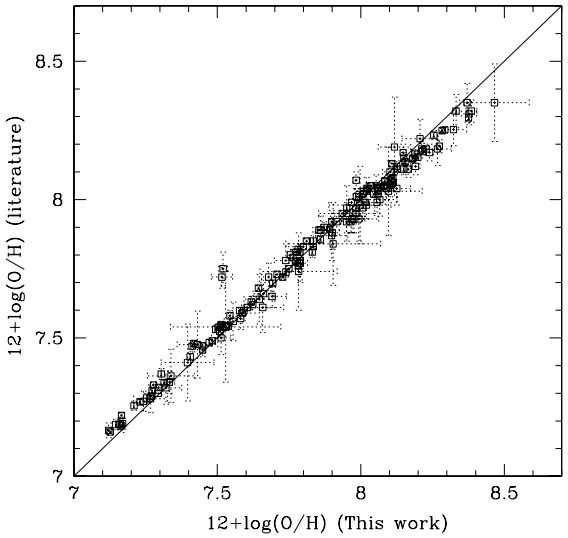

Fig. 1. Comparison between the T_e-based oxygen abundances (this work) and those from the literature.

3. Abundance determination from T_e

A two-zone model for the temperature structure within the H II region was adopted. In this model, T_e([O III]) is taken to represent the temperature for high-ionization species such as O^{++}, while T_e([O II]) is used for low-ionization species such as O^+. The general method is first to derive t_3 (=$10^{-4}T_e$([O III])) from the emission-line ratio of [O III]4959,5007/[O III]4363 and then to estimate t_2 (=$10^{-4}T_e$([O II])) from an analytical relation between t_2 and t_3 inferred from photoionization calculations.

Izotov et al. (2006) published a set of equations for the determination of the oxygen abundances in H II regions for a five-level atom. They used the atomic data from the references listed in Stasińska (2005). According to those authors, the electron temperature t_3 (in units of 10^4 K) and the ionic abundances O^{++}/H^+ and O^+/H^+ are estimated as follows:

$$t_3 = \frac{1.432}{\log((\lambda4959+\lambda5007)/\lambda4363) - \log C_T}, \quad (1)$$

where

$$C_T = \left(8.44 - 1.09t_3 + 0.5t_3^2 - 0.08t_3^3\right)\frac{1+0.0004x_3}{1+0.044x_3}, \quad (2)$$

with $x_3 = 10^{-4}n_e t_3^{-1/2}$, and n_e is the electron density in cm^{-3}. And

$$12+\log(O^{++}/H^+) = \log(I_{[OIII]\lambda4959+\lambda5007}/I_{H\beta}) + 6.200 + \frac{1.251}{t_3} - 0.55\log t_3 - 0.014t_3, \quad (3)$$

$$12+\log(O^{+}/H^+) = \log(I_{[OIII]\lambda3726+\lambda3729}/I_{H\beta}) + 5.961 + \frac{1.676}{t_2} - 0.40\log t_2 - 0.034t_2 + \log(1+1.35x_2), \quad (4)$$

with $x_2 = 10^{-4}n_e t_2^{-1/2}$, and n_e is the electron density in cm^{-3}. The total oxygen abundances are then derived from the following equation:

$$\frac{O}{H} = \frac{O^+}{H^+} + \frac{O^{++}}{H^+}. \quad (5)$$

The electron temperature t_2 (in units of 10^4 K) of the low-ionization zone is usually determined from t_3 following an equation derived by fitting H II region models. Several versions of this relation of t_2 vs. t_3 have been proposed. We used the one of Garnett (1992), which has been widely used:

$$t_2 = 0.7t_3 + 0.3. \quad (6)$$

The electron densities in the ionized gas of the galaxies were calculated from the line ratios [S II]λ6717/[S II]λ6731 by using the five-level statistical equilibrium model in the task TEMDEN contained in the IRAF/STSDAS package (de Robertis et al. 1987; Shaw & Dufour 1995), which uses the latest atomic data. A reasonable upper limit of the ratios is 1.431 (Osterbrock 1989). However, we find that 118 out of the 531 SDSS galaxies have [S II] line ratios higher than 1.431. For 71 of the 118 galaxies, the difference between the measured ratio and 1.431 is less than the error in the line ratio, so it is very possible that most of the high [S II]λ6717/[S II]λ6731 ratios come from errors. Therefore,

we adopt 1.431 for these galaxies. Indeed, this approximation would not affect the ionic abundances much. The reasons are: the term containing x_3 is never important and can be omitted in calculating C_T, since n_e is always smaller than 10^3 cm^{-3}, and x_2 is also insignificant since it is generally less than 0.1 with $n_e < 10^3$ cm^{-3}.

Oxygen abundances of all the 695 samples (531 from SDSS-DR4 and 164 from the literature) were estimated using the relations outlined above. The whole sample mostly shows a metallicity range of $7.1 < 12 + \log(O/H)_{T_e} < 8.5$. Most of the SDSS-DR4 galaxies lie in the more metal-rich region, i.e., $7.6 < 12 + \log(O/H)_{T_e} < 8.5$, and only 63 of them have lower metallicities than $12 + \log(O/H)_{T_e} = 8.0$. Most of the samples from the literature have lower metallicities, i.e., $12 + \log(O/H) < 8.0$. The typical uncertainty of the estimates is about 0.044 dex in 12+log(O/H) and about 500 K in T_e([O III]). All the data for the SDSS galaxies are given in Table 1.

4. Comparisons between the T_e and strong-line oxygen abundances

We compare the T_e-based O/H abundances of the sample galaxies with the Bayesian oxygen abundances provided by the MPA/JHU group, and those derived from other "strong-line" ratios, such as R_{23}, $R_{23} - P$, N2, and O3N2.

4.1. Comparison with the Bayesian metallicities obtained by the MPA/JHU group

The MPA/JHU group used photoionization model (Charlot et al. 2006) to simultaneously fit most prominent emission lines. Based on the Bayesian technique, they have calculated the likelihood distribution of the metallicity of each galaxy in the sample by comparing with a large library of models ($\sim 2 \times 10^5$) corresponding to different assumptions about the effective gas parameters, and then they adopted the median of the distribution as the best estimate of the galaxy metallicity (Tremonti et al. 2004; Brinchmann et al. 2004).

Very surprisingly, Fig. 2a shows that, for almost half of the sample galaxies (~227), their metallicities are overestimated by a factor of about 0.34 dex on average by using the model of Charlot et al. (2006). There is no obviously monotonic trend between the increasing discrepancy and the weakening [O III]4363 line or the decreasing [O III]4363/Hβ ratio. What is the reason for such obvious difference?

In fact, Charlot's model was based on Charlot & Longhetti (2001, CL01 hereafter), which is a model for consistently computing the line emission and continuum from galaxies, based on a combination of recent population synthesis and photoionization codes of CLOUDY. What they did is to use a sample of 92 local galaxies as the observed constraints to determine the best model parameters, including metallicity Z, etc. In their calibrations, they used the emission-line luminosities of Hα, Hβ, [O II]λ3727, [O III]λ5007, [N II]λ6583, and [S II]$\lambda\lambda$6717,6731 emission lines. The main difference between this method and the other strong line methods discussed below is that all the emission lines are used simultaneously so that any clear change in the abundance ratio X/O for any element X from that used in the CL01 models has the potential of causing offsets. In particular, the clear offset between $(O/H)_{Bay}$ and $(O/H)_{T_e}$ is possibly related to how secondary nitrogen enrichment is treated in the CL01 models.

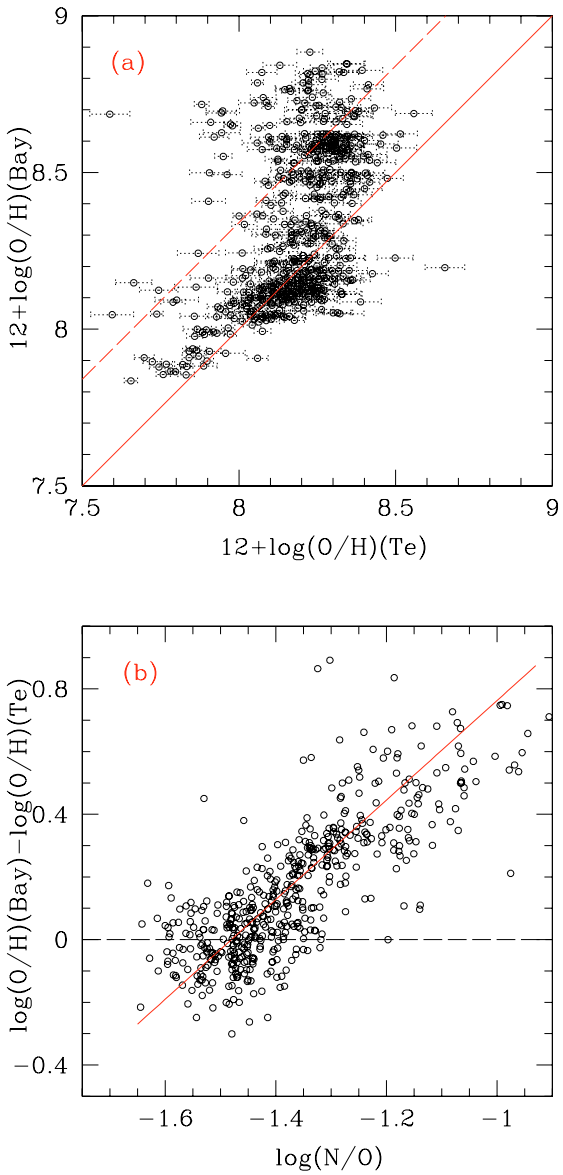

Fig. 2. a) Comparison between the electron temperature-based oxygen abundances and those Bayesian estimates obtained by the MPA/JHU group. The solid line is the equal-value line, and the long-dashed line represents a +0.34 dex discrepancy from the equal-value line to show the overestimates of the oxygen abundances by using the model of Charlot et al. (2006) for almost half of the sample galaxies. **b)** The offset between the $\log(O/H)_{Bay}$ and the $\log(O/H)_{T_e}$ as a function of the log(N/O) abundance ratios for the MPA/JHU sample galaxies. The solid line is the linear least-square fit for the relations, given as Eq. (7).

Figure 2b shows that the "offset" between $\log(O/H)_{Bay}$ and $\log(O/H)_{T_e}$ (the former minus the latter) strongly correlates with the log(N/O) abundance ratio, which can be shown as a linear least-square fit:

$$\text{offset} = 1.589 \times \log(N/O) + 2.352, \quad (7)$$

with an rms of 0.176 dex. The log(N/O) abundance ratios are obtained from the electron temperature in the [N II] emission region (equal to the t_2 given in Sect. 3) and the flux ratio of [N II]$\lambda\lambda$6548,6584 to [O II]λ3727 following the method given in Thurston et al. (1996). This means that the overestimates of CL01 models for the O/H abundances may be related to the onset of secondary N enrichment. There is a considerable spread in

the onset of N enrichment, so that the assumption of the CL01 models of a single N enrichment trend is too simplistic in this transition region. The simple way to avoid this problem might be to exclude [N II] from their fitting procedure. In this transition region, the relations between the log(N/O) and the log(O/H) of galaxies are not monotonic, unlike the almost constant trend in the low-metallicity region or the increasing trend in the high-metallicity region (see Fig. 8 of Liang et al. 2006).

4.2. R_{23} method

Pagel et al.(1979) first proposed the empirical abundance indicator R_{23} for metal-rich galaxies. Skillman et al. (1989) went on to suggest that this indicator can also be used for metal-poor galaxies. The relationship between O/H and R_{23} has been extensively discussed in the literature (see Tremonti et al. (2004) and references therein). Different calibrations will result in slightly different oxygen abundances even for the same branch (see Fig. 3 of Tremonti et al. 2004 for comparison). A few calibrations have attempted to improve the calibration by introducing an empirical estimator of the ionization parameter as a second parameter (e.g. McGaugh 1991; Charlot & Longhetti 2001; KD02 etc.). At present, one of the popular formulas is the calibration given by Kobulnicky et al.(1999), which includes two analytical formulas for the metal-rich and metal-poor branches, respectively, and is derived from the photoionization model of McGaugh (1991).

As mentioned in the introduction, R_{23} may overestimate the actual O/H abundances by a factor of ~0.2–0.5 dex (Kennicutt et al. 2003 etc.). On the basis of this large sample of 695 galaxies, we compare here their oxygen abundances derived from the R_{23} and T_e methods. Figures 3a and 3b show this comparison, where we use the calibration formula of Kobulnicky et al. (1999) to derive the $12+\log(O/H)_{R_{23}}$ for the sample galaxies. In Fig. 3a for the galaxies with $12+\log(O/H)_{T_e} < 7.95$, we use their calibration formula for metal-poor galaxies; and for the galaxies with $12+\log(O/H)_{T_e} \geq 8.2$, we use their formulas for the metal-rich branch. These two metallicity limits are defined following the $R_{23} - P$ method in Sect. 4.3 and some other related studies (Pilyugin 2000, 2001a,b; Shi et al. 2006). Figure 3a shows that the R_{23} method will overestimate the O/H abundances by a factor of ~0.20 dex, which is analogous to what was found by Kennicutt et al. (2003) and Shi et al. (2005, 2006). Detailed discussions of this discrepancy can be found in Kennicutt et al. (2003). For the sample galaxies with $8.0 < 12+\log(O/H)_{T_e} < 8.2$, which are in the turn-over region, the calibration in Kobulnicky et al. (1999) of metal-poor branch gives $(O/H)_{R_{23}}$ good agreement with $(O/H)_{T_e}$. These galaxies are omitted when we discuss the discrepancy between the T_e- and R_{23}-based metallicities, which is acceptable. Figure 3a does not show any obvious offset between the H II regions and galaxies. Pérez-Montero & Díaz (2005) show that the giant extragalactic H II regions (GEHRs) have more dispersion than the H II galaxies and H II regions in the Galaxy and the Magellanic clouds (their Figs. 1,3,7) since the GEHRs may have different ionization parameters and stellar effective temperatures.

To clearly illustrate the uncertainties due to the double-value of the R_{23}-O/H relation, we used both of the calibration formulas for metal-poor and metal-rich branches to calculate the $12+\log(O/H)_{R_{23}}$ abundances for the galaxies having $7.9 < 12+\log(O/H)_{T_e} < 8.4$. Figure 3b gives the results as the points between the two vertical dashed lines, which shows that these two different formulas will result in quite different metallicities, and the discrepancy may be up to ~0.4 dex. Therefore, one should be very careful when using the R_{23}-method to derive the metallicities of the galaxies having metallicities in the turn-over region.

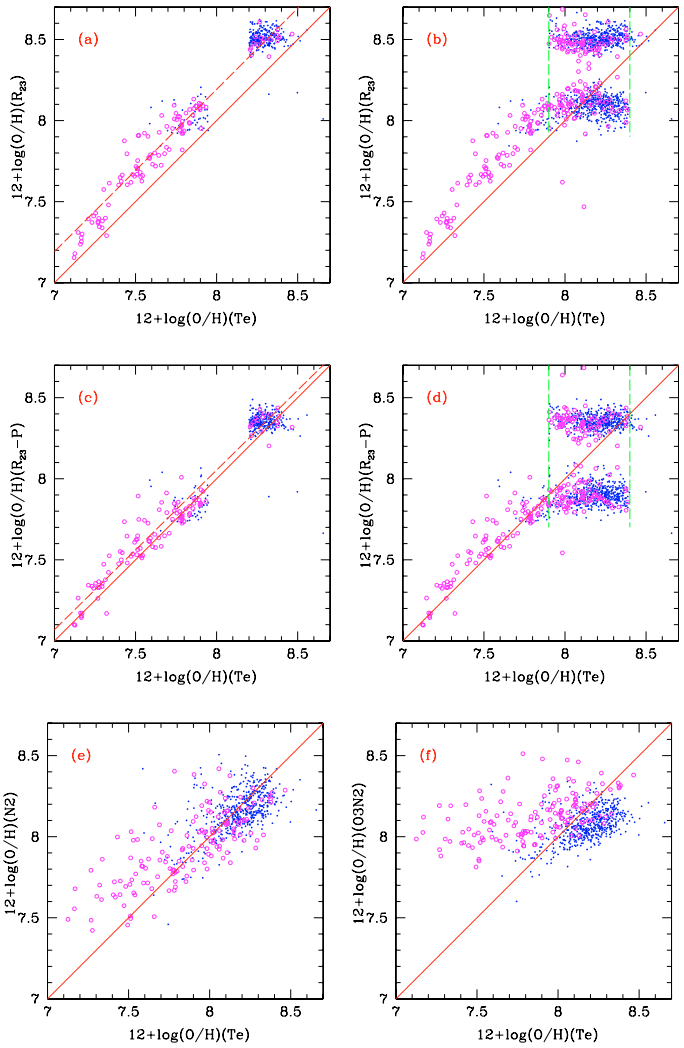

Fig. 3. Comparison between the T_e-based abundances with those derived from other strong-line calibrations: **a)**, **b)** R_{23} method; **c)**, **d)** $R_{23} - P$ method; **e)** N2 method; **f)** O3N2 method (see text). The small blue points represent the SDSS sample, and the larger magenta points (open circles) represent the sample compiled from the literature. The solid lines are the equal-value lines, and the long-dashed lines in **a)** and **c)** are the linear least-square fits to the data points, which show a discrepancy of ~0.20 dex and ~0.06 dex from the equal-value lines, respectively. The two pairs of vertical dashed lines in **b)** and **d)** show the range of $7.9 < 12+\log(O/H)_{T_e} < 8.4$ for the samples whose metallicities are estimated from strong-line ratios by using two calibrations for metal-rich and metal-poor branches.

4.3. The R_{23}-P method

Pilyugin (2000, 2001a,b) suggests that the P method estimates oxygen abundances of galaxies in which the oxygen abundance can be derived from two parameters, R_{23} and P (=[O III]/([O II]+[O III])). Therefore, we call this method the "$R_{23} - P$ method". They derived the $O/H = f(R_{23}, P)$ formulas from a sample of metal-poor H II regions with $7.1 < 12+\log(O/H)_{T_e} < 7.95$ and a sample of moderately metal-rich H II regions with $8.2 < 12+\log(O/H)_{T_e} < 8.7$. The best fitting relation for metal-poor objects is given as Eq. (4) in Pilyugin (2000), and the one for moderately metal-rich objects is given as Eq. (8) in Pilyugin (2001a).

Figure 3c shows that there is slight difference of ∼0.06 dex between the $(O/H)_{T_e}$ and the $(O/H)_{R_{23}-P}$ abundances for the samples. This good agreement is indeed not surprising since Pilyugin (2000, 2001a,b) derived the $R_{23} - P$ method formulas by using a subset of the sample we have used here (Izotov et al. 1994, 1997a; Izotov & Thuan 1998b, 1999). The minor offset is very likely caused for two reasons: (1) our larger sample than the one used by Pilyugin, which allowed us to determine the relations with higher precision; (2) the different T_e-formulas and/or atomic data used in calculations. Moreover, for the low excitation samples in the low-metallicity branch with $P < 0.75$, the $R_{23} - P$ method may overpredict their oxygen abundances by a factor ∼0.1 dex, which is consistent with the 0.1–0.2 dex overestimates found by van Zee & Haynes (2006) for the low-excitation H II regions in dwarf irregular galaxies.

Pilyugin & Thuran (2005) have renewed the $R_{23} - P$ calibrations by including several improvements, such as enlarging the sample by 1 order of magnitude, etc. We used the new calibrations to re-calculate the $(O/H)_{R_{23}-P}$ abundances for our sample galaxies and found the overstimate factor by the $R_{23} - P$ method decreases to ∼0.025 dex.

Because there are no observational samples with $7.95 < 12+\log(O/H) < 8.2$ in Pilyugin's calibration for the $R_{23} - P$ method, this method cannot provide information for the galaxies within this oxygen abundance range. To understand more about this, we calculated oxygen abundances for galaxies with $12+\log(O/H)_{T_e} = 7.9$–8.4 using the two formulas for the metal-rich and metal-poor branches. The results are indicated in Fig. 3d. Similar to what we saw for R_{23}, the two branch calibrations give quite different metallicities with a difference of up to ∼0.4 dex. Thus one must be very careful when applying the $R_{23} - P$ method to samples of galaxies with metallicities in the turn-over region.

4.4. N2 method

The [N II]/Hα emission-line ratio can also be used to estimate the metallicity of galaxies. Nitrogen is mainly synthesized in intermediate- and low-mass stars. The [N II]/Hα ratio will therefore become stronger with ongoing star formation and galaxy evolution, until very high metallicities are reached, i.e. $12+\log(O/H) > 9.0$, where [N II] starts to become weaker due to the very low electron temperature caused from strong cooling by metal ions. It is worth pointing out that this ratio gives an indirect measurement of the oxygen abundance, however, since oxygen lines are not used in the method.

Following the earlier work by Storchi-Bergmann et al. (1994), and Raimann et al. (2000), D02 and PP04 suggested calibration relations for O/H vs. N2 index from 236 and 137 galaxies respectively. D02 combined a sample of 128 metal-rich galaxies and 108 metal-poor galaxies with [O III]4363 detected to derive their calibration. The way they estimated the metallicities of their galaxy sample was to use the T_e-method for the metal-poor galaxies and the R_{23} or S_{23} (=log(([S II]6717,6731+[S III]9096,9531))/Hβ) method for the metal-rich ones. PP04 extracted the metal-poor objects from the work of D02 and updated the abundances for some of them with recent measurements by Kennicutt et al. (2003) for H II regions in M101 and by Skillman et al. (2003) for dwarf irregular galaxies in the Sculptor Group. To be consistent with the T_e-method, here we use the calibration formula given by PP04 to derive the metallicities $12+\log(O/H)_{N2}$ for our 695 sample galaxies. Figure 3e gives the comparison between the $12+\log(O/H)_{T_e}$ and $12+\log(O/H)_{N2}$, which shows that the two estimates are consistent but have some scatter. The scatter may mostly come from the different ionization parameters of the galaxies and the different samples (see Sect. 6.5).

One of the advantages of using the N2 index for estimating metallicity is that the N2 indicator can break the degeneracy when the $R_{23}-$ (O/H) and $(R_{23}, P)-$ (O/H) relations are double-valued. Also, the N2 index is not affected by dust extinction since Hα and [N II] are so closely spaced in wavelength. Furthermore, near-infrared spectrographs can measure these two lines for galaxies out to high redshifts, where it is equivalent to early epochs in the evolution of galaxies (see more discussion in Liang et al. 2006).

4.5. O3N2 method

Another indicator of the metallicity of galaxies is O3N2 (= $\log\{([O\,III]\lambda5007/H\beta)/([N\,II]\lambda6583/H\alpha)\}$). It was introduced by Alloin et al.(1979) and then studied by PP04, who present one such calibration by doing a linear least-square fit for a sample of 65 (from the 137) galaxies with $-1 < O3N2 < 1.9$, and provide a calibration formula. This calibration does not work for the cases of $O3N2 > 1.9$ since the data points are so scattered there in their study. Figure 3f shows the comparison between the $12+\log(O/H)_{T_e}$ and the oxygen abundances derived with the O3N2 method using the calibration of PP04 for our 695 sample galaxies. But we extrapolated to use the PP04's calibration to the galaxies with $O3N2 > 1.9$.

It is clear that this calibration will overestimate the O/H abundances by a big factor, up to 1.0 dex, for the metal-poor galaxies with O 3 N 2 > 1.9 (about $12+\log(O/H) < 8.0$). The scatter of the data with $-1 < O3N2 < 1.9$ is 4also large, which may be due to the different ionization parameters of the galaxies.

5. Comparisons with photoionization models

KD02 calculated the metallicity calibrations for strong-line ratios on the basis of photoionization models. They used a combination of stellar-population synthesis and photoionization models to develop a set of ionization parameters and abundance diagnostics based on emission-line ratios from strong optical lines, with seven ionization parameters $q = 5 \times 10^6$, 1×10^7, 2×10^7, 4×10^7, 8×10^7, 1.5×10^8, and 3×10^8 cm s^{-1}. The ionization parameter q is defined on the inner boundary of the nebula and can be physically interpreted as the maximum velocity of an ionization front that can be driven by the local radiation field. It will be interesting to compare the observational samples with these model results. Figure 4 shows the comparisons for the relations of $12+\log(O/H)$ versus R_{23}, N2, O3N2, and S2 indices. These relations are for the T_e-based oxygen abundances of the metal-poor galaxies. Liang et al. (2006) shows such relations for the metal-rich SDSS galaxies based on R_{23} abundances, and derived the corresponding calibrations (see Figs. 4b, c).

Figure 4a shows that the significant discrepancy in the theoretically expected R_{23} sequence with respect to the observed trend beginning from $12 + \log(O/H)_{T_e} = 8.0$ to lower metallicities. Nagao et al. (2006) also point this out. The observed relation of $R_{23} - \log(O/H)$ for the data points does not show much scatter in contrast to the models of the lower branch of metallicity, which may mean a weak dependence of R_{23} on ionization parameters there. In particular, the distribution of observational data is nearly vertical in an oxygen abundance range of 7.9 ∼ 8.5. The physical reason for the insensitivity of R_{23} to metallicity in this metallicity region is that the [O III]/Hβ ratio (also [O II]/Hβ) is

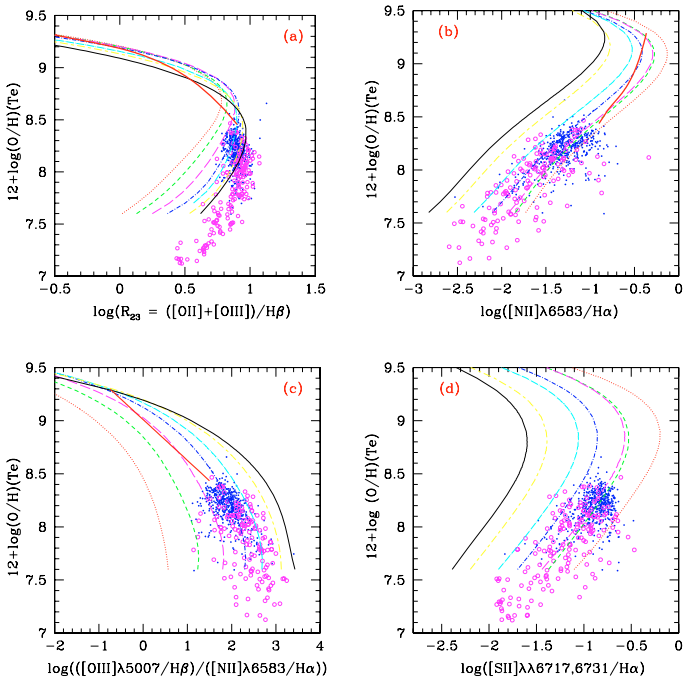

Fig. 4. Comparison between the observational data and the photoionization models of KD02. The symbols are the same as in Fig. 3. The seven lines represent the model results from KD02 with seven photoionization parameters from $q = 5 \times 10^6$ cm s^{-1} to $q = 3 \times 10^8$ cm s^{-1}, which increase in an orderly fashion from the red dotted line to the black solid line. The solid thick line (in red) in **a)** is the calibration derived by Tremonti et al. (2004) for the metal-rich galaxies, and those in **b)** and **c)** are the calibrations derived by Liang et al. (2006) for the metal-rich SDSS galaxies.

independent of T_e, there hence of metallicity (Stasinska 2002). It proves again that the oxygen abundance cannot be accurately measured by using R_{23} in the metallicity turnover region, but the R_{23} indicator works well for the metal-poor galaxies with 12 + log(O/H) < 7.9.

Figure 4b shows the comparison between 12+log(O/H) and the N2 index. It shows that the observational data follow the general trend of the model results closely; namely, the N2 indices of galaxies increase following the increasing metallicities, up to 12+log(O/H) = 9.0 (by models and Liang et al. 2006). The observational data show some scatter, which may be due to their different ionization parameters. We also plot the calibration relation derived by Liang et al. (2006) with the metal-rich SDSS galaxies (8.5 < 12 + log(O/H) < 9.3) in Fig. 4b. If we derive a calibration from the T_e-based oxygen abundances of the metal-poor galaxies and extrapolate it to the metal-rich region, it will result in relatively lower O/H abundance than when directly using the calibration from metal-rich galaxies. Perhaps one reason for this discrepancy stems from the different methods of determining metallicities of the metal-poor and metal-rich galaxies, i.e. the T_e-method versus the R_{23}-method, or photoionization models. However, Stasińska (2005) points out that, at high metallicity, the derived O/H values from T_e for model H II regions deviate strongly from the true ones; i.e., important deviations appear around 12 + log(O/H) = 8.6 and may become huge as the metallicity increases (see their Fig. 1a).

Figure 4c shows the comparison between 12+log(O/H) and the O3N2 index. The general trend of the observations and of the models is similar and shows increasing O/H abundance with decreasing O3N2 index. However, the large scatter of the data points in this plot may be due to the strong effect of the ionization parameter, and this effect is stronger in the low-metallicity region (12+log(O/H) < 8.5) than in the high-metallicity region (12+log(O/H) > 8.5). Moreover, O3N2 is much less dependent on metallicity in the low-metallicity region than in the high-metallicity region; in particular, it is almost independent of metallicity for the sample galaxies with metallicities of 12+log(O/H) = 7.1–7.7. This is possibly the main reason that PP04 had to limit their calibration to O3N2 < 1.9. We also present the calibration for metal-rich SDSS galaxies obtained by Liang et al. (2006) in Fig. 4c in the 8.5 < 12+log(O/H) < 9.3 region. Both the calibrations for the metal-rich and metal-poor sample galaxies are consistent with the general trend of the model predictions, but the calibration for metal-poor galaxies corresponds to relatively higher ionization parameter than the metal-rich galaxies.

Figure 4d shows the comparison between 12+log(O/H) and the S2 index. Both the observations and models clearly show increasing S2 with increasing O/H. This increasing trend will extend up to 12+log(O/H) ~ 8.9–9.0, but s2 is affected more by the ionization parameters than the N2 index is. The large scatter of this relation may be caused by the different ionization parameters. Most of the SDSS galaxies cluster around $-1.0 < S2 < -0.5$. Liang et al. (2006) did not derive a metallicity calibration for S2 for the metal-rich galaxies since the data points show obvious turnover and double-valued distribution around 12+log(O/H) ~ 8.9–9.0.

In summary, Figs. 4a–d show that R_{23} is not a good metallicity indicator for the galaxies with 7.9 < 12+log(O/H) < 8.5 due to its independence of metallicity there, and it is a good indicator of the lower metallicity region with 12+log(O/H) < 7.9; N2 is a useful indicator for estimating metallicities of galaxies because it is strongly monotonicly correlated with metallicity (up to about 12+log(O/H) ~ 9.0); although O3N2 and S2 can be used to estimate metallicities of galaxies, they are more sensitive to ionization parameters than N2 is, and O3N2 is less dependent on metallicity than the other two. In addition, when we have the indicator of O3N2 and/or S2, normally we also have N2. Furthermore, if we can find a way to take the ionization parameters of the sample galaxies into account in the calibrations, it will provide more reliable metallicities (see Sects. 6.5, 6.6).

6. Deriving oxygen abundance calibrations

We obtain the T_e-based O/H abundances for the 695 sample galaxies and H II region. They mostly have metallicities of $7.1 < 12 + \log(O/H)_{T_e} < 8.5$. Then, in this section, we use their $(O/H)_{T_e}$ and line ratios to re-derive the oxygen abundance calibrations for the N2, O3N2 indices, and add an S2 index. We also derive the calibration for R_{23} for the $12+\log(O/H)_{T_e} < 7.9$ region. Moreover, we try to add an excitation parameter P (=[O III]/([O II]+[O III])) in the calibrations to separate the sample galaxies to be three sub-samples, which improves the N2 calibration, but does not improve the O3N2 and S2 calibrations much.

6.1. The R_{23} index

The R_{23} index is useful for calibrating metallicities of low metallicity galaxies with 12+log(O/H) < 7.9 due to its obvious correlation with log(O/H) and weak dependence on ionization parameters there. Figure 5a shows this correlation. The linear

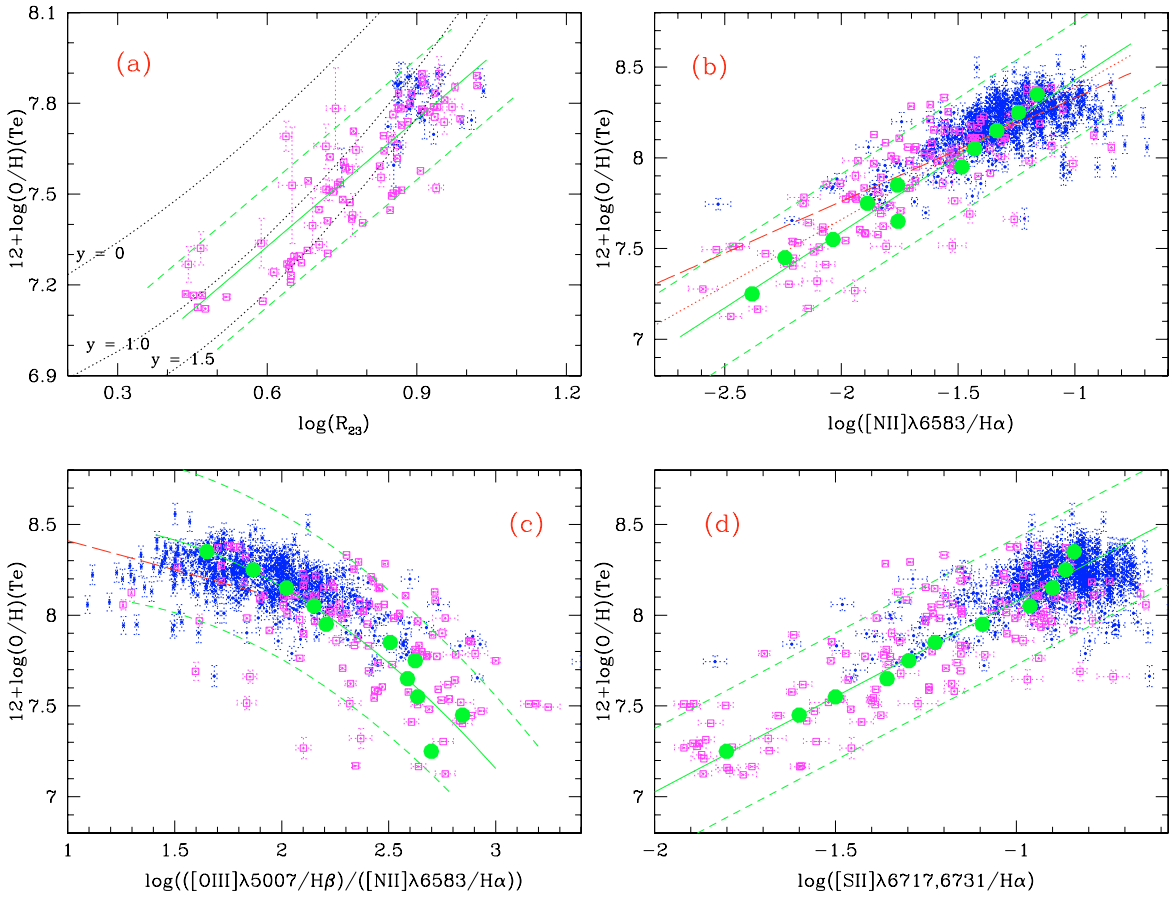

Fig. 5. R_{23}, N2, O3N2, and S2 indices for oxygen abundance calibrations from the sample galaxies: **a)** the R_{23} index; **b)** the N2 index; **c)** the O3N2 index; **d)** the S2 index. The small filled points represent the SDSS galaxies and the open squares refer to the samples from the literature. The points with uncertainties larger than 0.06 dex in all these line ratios and log(O/H) abundances have been excluded. The solid line **a)** refers to the linear least-square fit for all the 120 data points in the figure. The three dashed lines refer to the calibrations given by Kobulnicky et al. (1999) for the three different cases of y (=log([O III]/[O II])). In **b)**, the long-dashed and dotted lines refer to the calibrations of PP04 and D02, respectively. In **c)**, the long-dashed line refers to the calibration of PP04. In **b)**–**d)**, the 11 large filled circles represent the mean values in each bin of oxygen abundances (see text), and the solid lines are the least-square fits for these mean-value points. The two dashed lines show the 2σ discrepancy from the fits in all the four panels.

least-square fit for all the 120 data points with 12+log(O/H) < 7.9 is

$$12 + \log(\mathrm{O/H}) = 6.486 + 1.401 \times \log(R_{23}), \quad (8)$$

with R_{23} = ([O II]λ3727+[O III] $\lambda\lambda$4959,5007)/Hβ. The rms of the data to the fit is about 0.103 dex. The appropriate range of this calibration is about 0.4 < log(R_{23}) < 1.0 and 7.0 < 12+log(O/H) < 7.9. The calibrations of Kobulnicky et al. (1999) are also presented in the figure for comparison for the cases of y (=log([O III]/[O II])) equal to 0, 1, and 1.5. It shows that the y = 1.0 and 1.5 can usually explain these observational data.

6.2. The N2 index

Since the data points show a relatively tight linear relationship between N2 and 12+log(O/H), we obtain a linear least-square fit for this relation. We use the mean-value points in 11 bins of metallicities to avoid too much weight in the high metallicity range where most of the data are distributed. The bin width is Δ[log(O/H)] = 0.1 for the galaxies in the range of 7.4 < 12+log(O/H) < 8.5, and Δ[log(O/H)] = 0.3 for the range of 7.1 < 12 + log(O/H)$_{T_e}$ < 7.4 because of the small number of sources in this range. These bin widths are the same as for the O3N2 and S2 indices discussed in the consequent two subsections. The objects with higher uncertainty than 0.06 dex on log(O/H) and log([N II]/Hα) have been excluded in calculating the mean values and calibrating, which leaves 584 data points. Nineteen galaxies from the literature cannot be included in deriving calibrations since they do not have [N II] emission-line measurements. The derived analytical relation of a linear least-square fit is

$$12 + \log(\mathrm{O/H}) = 9.263 + 0.836 \times \mathrm{N2}, \quad (9)$$

with N2 = log([N II]λ6583/Hα), shown in Fig. 5b. The rms of the data to the fit is 0.159 dex. A 2σ discrepancy is shown by the two dashed lines. This calibration is valid in the range of −2.5 < N2 < −0.5. The calibrations of D02 (12 + log (O/H) = 9.12 + 0.73× N2) and PP04 (12 + log (O/H) = 8.90 + 0.57× N2) are also plotted for comparison. It shows that D02's calibration is similar to ours, but the one of PP04 shows a slightly lower slope and the difference is more obvious for the low metallicity region with 12+log(O/H) < 8.0. The reason may be that PP04's sample does not extend to much lower metallicity with 12+log(O/H) < 7.7, and most of their samples have metallicities of 7.7 < 12+log(O/H) < 8.5, while the fit for their these samples results in a slightly lower slope than for ours (see Fig. 1 of D02 and Fig. 1 of PP04).

6.3. The O3N2 index

Figure 5c shows our sample galaxies for their $(O/H)_{T_e}$ abundances versus O3N2 indices. Although they are quite scattered, an obvious trend still exists; i.e., O/H increases following the decreasing O3N2 index. We tried to derive a calibration of O3N2 index for O/H abundances from these sample galaxies. The objects with an higher uncertainty than 0.06 dex on log(O/H) and O3N2 are excluded, which leaves 585 data points. Nineteen objects from the literature without their [N II] emission-line measurements are excluded. The mean-value points within 11 bins are obtained for the left sample galaxies. The bin widths are the same as for the N2 calibration (Sect. 6.2). A two-order polynomial fit is obtained by fitting the mean-value points

$$12 + \log(O/H) = 8.203 + 0.630 \times O3N2 - 0.327 \times O3N2^2, \quad (10)$$

with O3N2 = log[([O III]λ5007/Hβ)/([N II] λ6583/Hα)], shown in Fig. 5c. The rms of the data to the fit is 0.199 dex. This fit is valid for 1.4 <O3N2 < 3. The 2σ discrepancy is shown by the two dashed lines. The calibration of PP04 ($12 + \log(O/H) = 8.73 - 0.32 \times O3N2$) is only valid for $1 < O3N2 < 1.9$. The calibration of PP04 shows a shallower slope than ours, which comes from their much smaller sample (65 objects) and the much narrower O3N2 range.

6.4. The S2 index

The S2 index (log([S II]$\lambda\lambda$6717,6731/Hα)) is also a metallicity-sensitive indicator. Although it is less useful than N2 for metallicity calibration due to the stronger dependence on the ionization parameter, it is still interesting to derive a calibration from S2 since it is dependent on metallicity monotonicly in the studied metallicity range. This relation has the advantage of not being strongly dependent on reddening corrections. Although the sample data is very scattered, a linear relation obviously exists between O/H and S2.

We calculated the mean values of S2 and O/H abundances for the sample galaxies in 11 bins, the bin widths are the same as we used for the N2 and O3N2 calibrations. Again, the objects with a higher uncertainty than 0.06 dex on log(O/H) and log([S II]/Hα) are excluded in the calculations, which leaves 607 data points. A least-square linear fit to the mean-valued points yields the relation:

$$12 + \log(O/H) = 9.128 + 1.051 \times S2, \quad (11)$$

with S2 = log([S II]$\lambda\lambda$6717,6731/Hα), shown in Fig. 5d. The rms of the data to the fit is about 0.176 dex. The 2σ discrepancy is shown by the two dashed lines.

6.5. Add the P parameter

The calibration of O/H vs. N2 is dependent on the ionization parameter (Fig. 4b), as well the O3N2 and S2 indices (Figs. 4c, d). Therefore, to get more reliable O/H abundances, an excitation parameter could be included in the calibrations, which correlates strongly with ionization parameter and the hardness of the ionizing radiation field. We use the P parameter given by Pilyugin (2000, 2001a,b), where P was defined as [O III]/([O II]+[O III]), which is similar to [O III]/[O II], the excitation parameter used by Kobulnicky et al. (1999) in calibrations. We should notice that P needs to be computed from the dereddened emission lines.

In Fig. 6a, we plot the $(\log(O/H)_{T_e} - \log(O/H)_{N2})$ vs. P relations for the sample galaxies, which shows that these galaxies

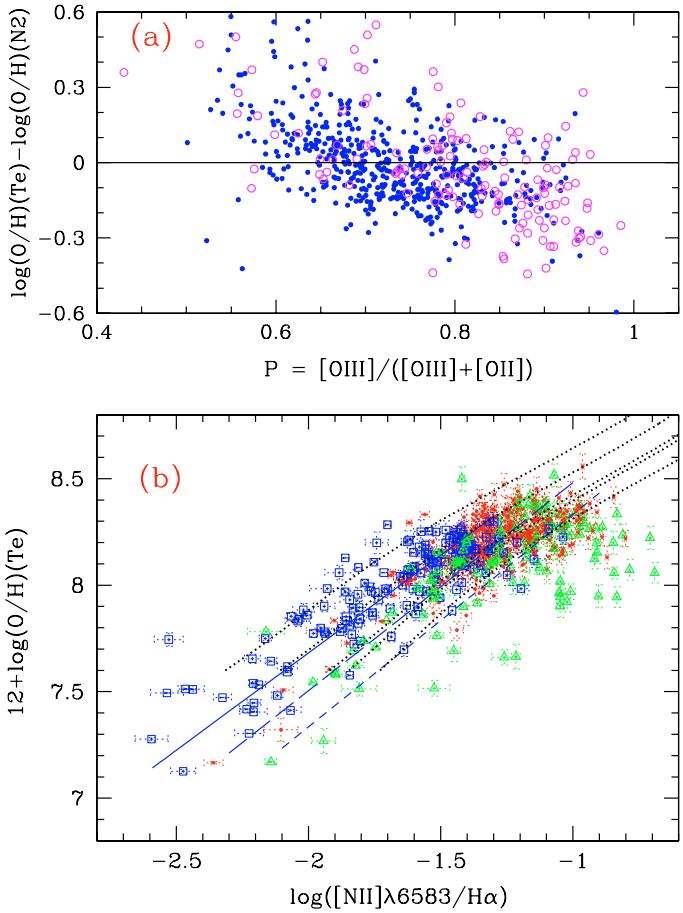

Fig. 6. a) The relation between $\log(O/H)_{T_e} - \log(O/H)_{N2}$ vs. P for the sample galaxies, which shows that they can be roughly divided into three subsamples with different P parameters: $P > 0.80$, $0.65 < P < 0.80$ and $P < 0.65$. The symbols are the same as in Fig. 4. **b)** The calibration of N2 index together with the P parameter. The blue open squares represent the samples with $P > 0.80$, the red points represent those with $0.65 < P < 0.80$, and the green triangles represent those with $P < 0.65$. The solid, long-dashed, and short-dashed lines refer to the linear least-square fits for each of the three subsamples, respectively (Eq. (12)). The five dotted lines are the model results of KD02, from the right to the left ones, the ionization parameter q increases from the 5×10^6 to the 1×10^7, 2×10^7, 4×10^7, and 8×10^7 cm s^{-1} grids.

can be roughly separated into three subsamples with $P < 0.65$ (143 data points), $0.65 < P < 0.80$ (292 data points), and $P > 0.80$ (149 data points). We derive the N2 calibrations for these three subsamples individually. The analytical calibrations of linear least-square fits for the three subsamples with different P parameters are:

$$\begin{aligned} 12 + \log(O/H) &= 9.514 + 0.916 \times N2, \quad (P > 0.80), \\ &= 9.457 + 0.976 \times N2, \quad (0.65 < P < 0.80), \\ &= 9.332 + 0.998 \times N2, \quad (P < 0.65). \end{aligned} \quad (12)$$

The rms of the data to each fit are 0.150, 0.140, and 0.189 dex, respectively. The dotted lines are the photoionization model results of KD02. It shows that the three different P values only correspond to the cases of KD02 of $q = 4 \times 10^7$, 1×10^7(as well 2×10^7), and 5×10^6 cm s^{-1}.

We also tried to add P as an additional parameter for the O3N2 and S2 indices. The sample galaxies are separated into three sub-samples with $P < 0.60$, $0.60 < P < 0.85$, and $P > 0.85$ to derive calibrations for these two indices. The basic

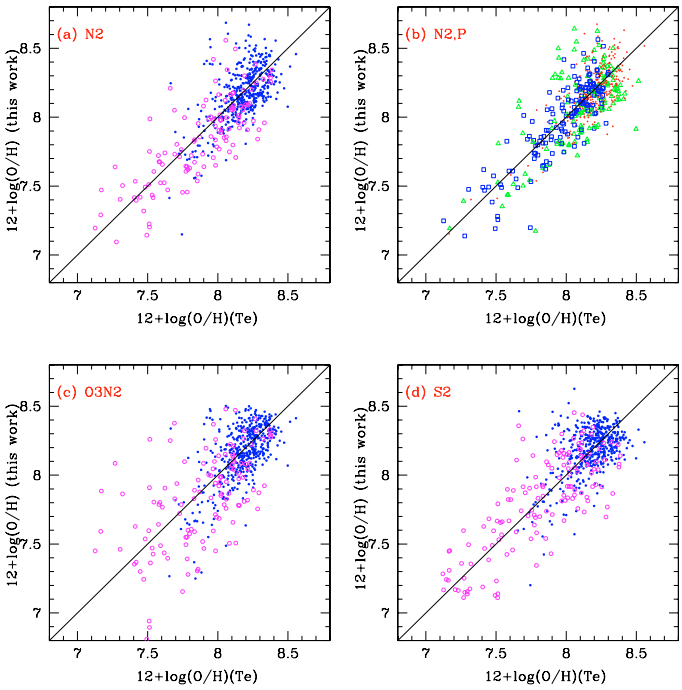

Fig. 7. Comparisons between the T_e-based O/H abundances with those derived from strong-line ratios, including N2 (without and with P), O3N2, and S2 indices: **a)** for the N2 index (without P, Eq. (9), Fig. 5b); **b)** for the N2 index (with P, Eq. (12), Fig. 6); **c)** for the O3N2 index (Eq. (10), Fig. 5c); **d)** for the S2 index (Eq. (11), Fig. 5d). The rms values of the data to the equal-value lines in each plot are 0.162, 0.158, 0.191, and 0.171 dex, respectively, and they will increase to 0.173, 0.167, 0.215, and 0.203 dex if the data points with uncertainties larger than 0.06 dex in line indices and log(O/H) are included. The symbols in **a)**, **c)**, **d)** are the same as in Fig. 4, and the symbols in **b)** are the same as in Fig. 6b.

results consistently follow the photoionization models of KD02. However, we find adding a P parameter does not improve the fits much. Therefore, we do not present the two-parameter calibrations for the O3N2 and S2 indices as figures here. We should note that using P with [N II]/Hα means that we need observations covering a much wider wavelength range, which might not be practical at high z. It is not necessary to add the P parameter to the R_{23} calibration since the observational data in the R_{23} vs. O/H relation does not show obvious dependence on ionization parameter in contrast to the lower-branch models (Fig. 4a).

6.6. The accuracies of the derived calibrations

We have presented the least-square fits for the relations of 12 + log(O/H)$_{T_e}$ and $N2$, $O3N2$, and $S2$ indices with and without considering the P excitation parameter. To show the accuracies of these calibrations, in Figs. 7a–d we plot the comparisons between log(O/H)$_{T_e}$ and those from line indices. Figures 7a,c,d show the comparisons with the calibrated abundances from N2, O3N2, S2 indices following Eqs. (9)–(11), which have been given as the solid lines in Figs. 5b–d, respectively. Figure 7b shows the calibrated abundances from the N2 index but adding the P parameter following Eq. (12), which improved the N2 calibration. Among these, the rms of the O3N2 and S2 calibrations are large, about 0.191 and 0.171 dex respectively (Fig. 7c,d). The calibration of (N2,P) case (Fig. 7b) shows the lowest rms, which is about 0.158, a bit lower than the rms in Figs. 7a and 3e for the N2 calibration (0.162 and 0.160 dex respectively).

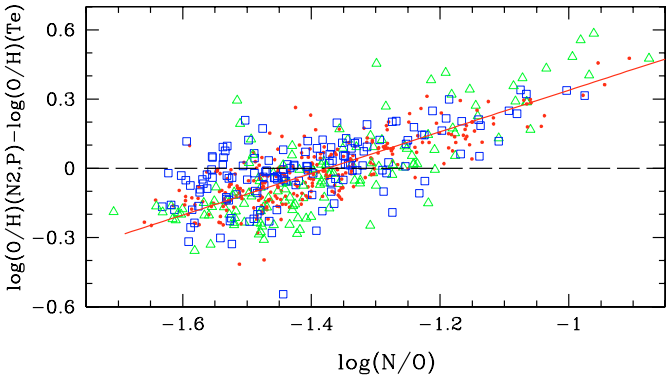

Fig. 8. Correlation between the difference in log(O/H)$_{N2,P}$ and log(O/H)$_{T_e}$ and the log(N/O) abundance ratios of the sample galaxies. The symbols are the same as in Figs. 6b, 7b. The solid line is the linear least-square fit for the relations with an rms of 0.104 dex.

Some of the remaining scatter in log(O/H)$_{N2,P}$ may come from the different star-forming history and evolutionary status of the sample galaxies. Figure 8 shows a clear correlation between the log(O/H)$_{N2,P}$ − log(O/H)$_{T_e}$ and the log(N/O) abundance ratios of the sample galaxies, which can be given as a linear least-square fit:

$$\log(\mathrm{O/H})_{N2,P} - \log(\mathrm{O/H})_{T_e} = 0.902 \times \log(\mathrm{N/O}) + 1.240, \quad (13)$$

with an rms of 0.104 dex. The corrected calibration of ($N2$, P) by considering this correlation will provide more accurate oxygen abundance, and the rms of the data to the equal-value lines in Figs. 7a and 7b will decrease to 0.115 dex, which is much less than the previous ones (0.162 and 0.158 dex, respectively). This correlation can be used to correct the derived oxygen abundances from the strong-line ratio when it is necessary. Nevertheless, to apply the N/O correction to 12+log(O/H) abundances, we need to measure [O II], [O III], and Hβ, in addition to [N II] and Hα, so it will not always be practical.

We should notice that both the x and y axes of Fig. 8 depend on nitrogen abundance, which means that the observed correlation could be spurious if the errors in log(N) are large. However, the errors in the log(N/O) abundances of the sample galaxies are quite small. It is about 0.011 dex on average for the MPA/JHU sample galaxies, which is expected since we only select the objects with higher signal-to-noise ratio, i.e. larger than 5σ, on the flux measurements of [N II] (see Sect. 2.1). For other samples from the literature, the errors in their log(N/O) values are about 0.021 dex on average. Therefore, this correlation is robustly measured and could be used to correct 12+log(O/H)$_{\mathrm{N2,P}}$ measurements if desired. More important, the strong trend in Fig. 8 highlights the sensitivity of the N2 calibration to a galaxy's *past* history of star formation, since it determines the present-day N/O ratio.

7. Conclusions

We compiled a large sample of 695 low-metallicity galaxies and H II regions with [O III]4363 detected, which consists of 531 galaxies from the SDSS-DR4 and 164 galaxies and H II regions from the literature. We determined their electron temperatures, electron densities, and then the T_e-based oxygen abundances. The derived oxygen abundances for them are 7.1 < 12+log(O/H) < 8.5.

The comparison of the T_e-based oxygen abundances and the Bayesian metallicities obtained by the MPA/JHU group show that, for about half of the MPA/JHU sample galaxies in this study, their O/H abundances were overestimated by a factor of 0.34 dex on average by using the photoionization models (Charlot et al. 2006; Tremonti et al. 2004; Brinchmann et al. 2004). This is possibly related to how secondary nitrogen enrichment is treated in the models they used.

The T_e-derived oxygen abundances of these sample galaxies were compared with those derived from other strong-line ratios, such as R_{23}, $R_{23} - P$, N2, and O3N2 indicators. The results show that the R_{23} and $R_{23} - P$ methods will generally overestimate the oxygen abundances of the sample galaxies by a factor of ∼0.20 dex and ∼0.06 dex, respectively. This 0.06 dex discrepancy is quite small, and will decrease to 0.025 dex when the improved $R_{23}-P$ calibrations given by Pilyugin & Thuan (2005) are used. The abundance calibration of N2 index, rather than O3N2 index, from PP04 can result in consistent O/H abundances with $(O/H)_{T_e}$ but with a scatter of about 0.16 dex.

From this large sample of 695 star-forming galaxies and H II regions, we re-derive abundance calibrations for R_{23}, N2, O3N2, and S2 indices on the basis of their oxygen abundances derived from T_e. The N2, O3N2, and S2 indices monotonicly change following the increasing O/H abundances from 12+log(O/H) = 7.1 to 8.5, which are consistent with the photoionization model results of KD02. The R_{23} parameter is a good metallicity indicator for the metal-poor galaxies with 12+log(O/H) < 7.9. Nevertheless, R_{23} does not follow the KD02 models well.

The scatter of the observational data may come from the differences in the ionizing radiation field. We add an excitation parameter P to separate the sample galaxies into three sub-samples, and then re-derive the N2 calibrations with three different P cases (<0.65, 0.65–0.80, >0.80), which improves the calibration, confirmed by the decreasing rms of the data to the equal-value line, which decreases from 0.162 in Fig. 7a to 0.158 in Fig. 7b. Adding the P parameter in the O3N2 and S2 indices does not improve the calibrations. However, some of the remaining scatter in the (N2,P) calibration may come from the different star-forming history and evolutionary status of the galaxies, which can be confirmed by the correlation between the $\log(O/H)_{N2,P} - \log(O/H)_{T_e}$ and log(N/O) of them (Fig. 8 and Eq. (13)).

In future studies of the calibrating oxygen abundances of galaxies, when their T_e values are not available, we can use the R_{23}, N2, O3N2, or S2 indices, together with the P parameter if the wavelength coverage is wide enough, to calibrate their oxygen abundances. The R_{23} parameter shows obvious correlation with oxygen abundances for the low-metallicity galaxies with 12+log(O/H) < 7.9. Compared with O3N2 and S2, The N2 index is less affected by ionization parameter and more obviously correlated with O/H abundances. Also it can be detected by the near-infrared instruments for the intermediate- and high-z star-forming galaxies. The N2 index has helped to provide important information on the metallicities of galaxies at high-z; for example, see Shapley et al. (2004) for a sample of 7 star-forming galaxies at $2.1 < z < 2.5$, Shapley et al. (2005) for a sample of 12 star-forming galaxies at $z \sim 1.0$–1.5, and Erb et al. (2006) for the six composited spectra of 87 rest-frame UV-selected star-forming galaxies at $z > 2$, etc. However, considering the dependence of N2, as well as the (N2,P) calibration on log(N/O) shown as Fig. 8, we should keep in mind that the resulting log(O/H) abundances from N2 may involve the specific history of N-enrichment in the galaxies. We may worry a bit about comparing the low and high-z observations using [N II] for this reason.

Given the good consistency of our N2 and S2 abundance calibrations with the models of KD02 at low metallicity (see Fig. 4b,d), it may be appropriate to linearly extrapolate our calibrations up to the high metallicity region, up to 12+log(O/H)∼9.0 and 8.8 respectively. However, this extrapolation on N2 will result in a lower log(O/H) abundance than the one directly derived from the calibration of the metal-rich SDSS galaxies obtained by Liang et al. (2006), which may be due to the discrepancy between the T_e- and the R_{23}-based metallicities. However, the T_e-based O3N2 calibration cannot be directly extrapolated to the metal-rich region since the slopes of the correlation relations between log(O/H) vs. O3N2 are not the same in the high-metallicity branch as in the low-metallicity branch (Fig. 4c). The R_{23} parameter cannot provide reliable oxygen abundances for the galaxies in the metallicity turn-over region with 7.9 < 12+log(O/H) < 8.4.

Acknowledgements. We thank the referee for many valuable and wise suggestions and comments, which helped us in improving this work. We thank Stephane Charlot for the interesting discussions about their models for estimating the oxygen abundances of the SDSS galaxies. S.Y.Y. and Y.C.L. thank Jing Wang and Caina Hao for the interesting discussions about the SDSS database. S.Y.Y thanks Yongheng Zhao and the LAMOST group for kindly providing their office for his stay. This work was supported by the Natural Science Foundation of China (NSFC) Foundation under No.10403006, 10433010 10373005, 10573022, 10333060, and 10521001.

References

Adelman-McCarthy, J. K., et al. 2006, ApJS, 162, 38
Alloin, D., Collin-Souffrin, S., Joly, M., & Vigroux, L., 1979, A&A, 78, 200
Baldwin, J., Phillips, M. M., & Terlevich, R. J. 1981, PASP, 93, 5
Bresolin, F., Garnett, D. R., & Kennicutt, R. C. Jr. 2004, ApJ, 615, 228
Bresolin, F., Schaerer, D. et al. 2005, A&A, 441, 981
Brinchmann, J., Charlot, S., White, S. D. M., et al. 2004 MNRAS, 351, 1151
Bruzual, A. G., & Charlot, S. 2003, MNRAS, 344, 1000
Calzetti, D., Kinney, A. L., & Storchi-Bergmann, T. 1994, ApJ, 429, 582
Charlot, S., & Longhetti, M. 2001, MNRAS, 323, 887 (CL01)
de Robertis, M. M., Dufour, R. J., & Hunt, R. W. 1987, JRASC, 81, 195
Denicoló, G., Terlevich, R., & Terlevich, E. 2002, MNRAS, 330, 69 (D02)
Díaz, A. I., Terlevich, E., Vílchez, J. M., Pagel, B. E., & Edmunds, M. G., 1991, MNRAS, 253, 245
Erb, D. K., Shapley, A. E., Pettini, M., et al. 2006, ApJ, 644, 813
Garnett, D. R. 1992, AJ, 103, 1330
Garnett, D. R., Edmunds, M. G., Henry, R. B. C., Pagel, B. E. J., & Skillman, E. D. 2004a, AJ, 128, 2772
Garnett, D. R., Kennicutt, R. C. Jr., & Bresolin, F. 2004b, ApJ, 607, 21
Guseva, N. G., Papaderos, P., Izotov, Y. I., et al. 2003a, A&A, 407, 75
Guseva, N. G., Papaderos, P., Izotov, Y. I., et al. 2003b, A&A, 407, 91
Guseva, N. G., Papaderos, P., Izotov, Y. I., et al. 2003c, A&A, 407, 105
Izotov, Y. I., & Thuan, T. X. 1998a, ApJ, 497, 227
Izotov, Y. I., & Thuan, T. X. 1998b, ApJ, 500, 188
Izotov, Y. I., & Thuan, T. X. 1999, ApJ, 511, 639
Izotov, Y. I., & Thuan, T. X. 2004, ApJ, 602, 200
Izotov, Y. I., Thuan, T. X., & Lipovetsky, V. A., 1994, ApJ, 435, 647
Izotov, Y. I., Andrew, B. D., et al. 1996, ApJ, 458, 524
Izotov, Y. I., Thuan, T. X., & Lipovetsky, V. A. 1997a, ApJS, 108, 1
Izotov, Y. I., Lipovetsky, V. A., et al. 1997b, ApJ, 476, 698
Izotov, Y. I., Chaffee, F. H., Foltz, R. F., et al., T. X., 1999, ApJ, 527, 757
Izotov, Y. I., Chaffee, F. H., & Green, R. F. 2001a, ApJ, 562, 727
Izotov, Y. I., Chaffee, F. H., & Schaerer, D. 2001b, A&A, 378, 45
Izotov, Y. I., Papaderos, P., Guseva, N. G., Fricke, K. J., & Thuan, T. X., 2004, A&A, 421, 539
Izotov, Y. I., Stasinska, G., Meynet, G., Guseva, N. G., & Thuan, T. X. 2006, A&A, 448, 955
Kauffmann, G., Heckman, T. M., Tremonti, C., et al. 2003, MNRAS, 346, 1055
Kennicutt, R. C. Jr., 1992, ApJ, 388, 310
Kennicutt, R. C. Jr., Bresolin, F., & Garnett, D. R. 2003, ApJ, 591, 801
Kewley, L. J., & Dopita, M. A. 2002, ApJS, 142, 35 (KD02)
Kewley, L. J., Dopita, M. A., Sutherland, R. S., Heisler C. A., & Trevena, J. 2001, ApJ, 556, 121
Kewley, L. J., Jansen, R. A., & Geller, M. J. 2005, PASP, 117, 227

Kinney, A. L., Bohlin, R. C., Calzetti, D., Panagia, N., & Wyse, R. F. G., 1993, ApJS, 86, 5
Kniazev, A. Y., Pustilnik, S. A., Masegosa, J., et al. 2000, A&A, 357, 101
Kobulnicky, H. A., Kennicutt, R. C. Jr., & Pizagno, J. L. 1999, ApJ, 514, 544 (K99)
Lamareille, F., Contini, T., Brinchmann, J., et al. 2006, A&A, 448, 907
Lee, J. C., Salzer, J. J., & Melbourne, J. 2004, ApJ, 616, 752
Liang, Y. C., Yin, S. Y., Hammer, F., et al. 2006, ApJ, 652, 257
McGaugh, S. S. 1991, ApJ, 380, 140
Melbourne, J., Phillips, A., Salzer, J. J., Gronwall, C., & Sarajedini, V. l. 2004, AJ, 127, 686
Moustakas, J., & Kennicutt, R. C.Jr. 2006, ApJ, 651, 155
Nagao, T., Maiolino, R., & Marconi, A. 2006, A&A, 459, 85
Osterbrock, D. E. 1989, Astrophysics of Gaseous Nebulae and Active Galactic Nuclei (Mill Valley, California: University Science Books)
Pagel, B. E. J., Edmunds, M. G., Blackwell, D. E., et al. 1979, MNRAS, 189, 95
Pettini, M., & Pagel, B. E. J. 2004, MNRAS, 348, L59 (PP04)
Pérez-Montero, E., & Díaz A. I. 2005, MNRAS, 361, 1063
Pilyugin, L. S. 2000, A&A, 362, 325
Pilyugin, L. S. 2001a, A&A, 369, 594
Pilyugin, L. S. 2001b, A&A, 373, 56
Pilyugin, L. S., & Thuan, T. X. 2005, ApJ, 631, 231
Pilyugin, L. S., Contini, T., Vílchez, J. M. 2004, A&A, 423, 427
Pilyugin, L. S., Thuan, T. X., & Vílchez, J. M. 2006, MNRAS, 367, 1139
Raimann, D., Storchi-Bergmann, T., Bica, E., et al. 2000, MNRAS, 316, 559
Shapley, A. E., Erb, D. K., Pettini, M., et al. 2004, ApJ, 612, 108
Shapley, A. E., Coil, A. L., Ma, C. P., & Bundy, K. 2005, ApJ, 635, 1006
Shaw, R. A., & Dufour, R. J., 1995, PASP, 107, 896
Shi, F., Kong, X., Li, C., & Cheng, F. Z. 2005, A&A, 437, 849
Shi, F., Kong, X., & Cheng, F. Z. 2006, A&A, 453, 487
Skillman, E. D., Kennicutt, R. C. Jr., & Hodge, P. W., 1989, ApJ, 347, 875
Skillman, E. D., Cote, S., & Miller, B. W. 2003, AJ, 125, 610
Stasińska, G. 2002, Lectures to be published in the proceedings of the XIII Canary Islands Winter School of Astrophysics, [arXiv:astro-ph/0207500]
Stasińska, G. 2005, A&A, 434, 507
Stasińska, G., & Leitherer C. 1996, ApJS, 107, 661
Storchi-Bergmann, T., Calzetti D., & Kinney A. L. 1994, ApJ, 429, 572
Thurston, T. R., Edmunds, M. G., & Henry, R. B. C. 1996, MNRAS, 283, 990
Tremonti, C. A., Heckman, T. M., Kauffmann, G., et al. 2004, ApJ, 613, 898
van Zee, L. 2000, ApJ, 543, L31
van Zee, L., & Haynes, M. P. 2006, ApJ, 636, 214
Veilleux, S., & Osterbrock, D. 1987, ApJS, 63, 295
Vílchez, J. M., & Iglesias-Páramo, J. 2003, ApJS, 145, 225

Online Material

Table 1. The characteristic parameters of the SDSS galaxies: N2 = log([N II]6483/Hα), O3N2 = log(([O III]5007/Hβ)/([N II]6483/Hα)), S2 = log([S II]6717,6731/Hα), P = [O III]/([O II]+[O III]). $(O/H)_{Bay}$ = 12+$(O/H)_{Bayesian}$ obtained by the MPA/JHU group.

(1)	(2)	(3)	(4)	(5)	(6)	(7)	(8)	(9)	(10)
Num	Plate-MJD-FiberID	IAU designations	t_3 (10^4K)	$12+(O/H)_{T_e}$	$(O/H)_{Bay}$	N2	S2	O3N2	P
1	266- 51630- 407	J094333.91+010659.4	1.080 ± 0.062	8.197 ± 0.050	8.659	–0.911 ± 0.005	–0.683 ± 0.005	1.436 ± 0.003	0.552
2	270- 51909- 617	J101430.99+004754.9	1.198 ± 0.037	8.141 ± 0.031	8.427	–1.331 ± 0.010	–0.954 ± 0.011	2.128 ± 0.008	0.776
3	276- 51909- 490	J105342.55+000945.0	1.203 ± 0.073	8.142 ± 0.051	8.179	–1.250 ± 0.014	–0.746 ± 0.009	1.941 ± 0.012	0.639
4	277- 51908- 451	J110116.39+004814.4	1.450 ± 0.029	7.982 ± 0.025	8.090	–1.605 ± 0.026	–1.346 ± 0.029	2.581 ± 0.024	0.924
5	282- 51658- 543	J113703.79+002817.4	1.199 ± 0.025	8.210 ± 0.022	8.206	–1.413 ± 0.014	–0.918 ± 0.008	2.303 ± 0.012	0.811
6	283- 51959- 572	J114649.34+005345.9	1.608 ± 0.035	7.884 ± 0.030	7.990	–2.019 ± 0.041	–1.392 ± 0.022	3.018 ± 0.033	0.937
7	285- 51930- 154	J120047.07-003611.8	1.056 ± 0.067	8.311 ± 0.061	8.234	–1.247 ± 0.010	–0.769 ± 0.009	1.947 ± 0.008	0.656
8	289- 51990- 369	J122419.73+010559.6	1.245 ± 0.033	8.075 ± 0.027	7.993	–1.615 ± 0.014	–1.019 ± 0.009	2.419 ± 0.012	0.809
9	292- 51609- 372	J124715.31+003806.7	1.235 ± 0.048	8.099 ± 0.032	8.087	–1.362 ± 0.011	–0.774 ± 0.007	2.077 ± 0.009	0.679
10	296- 51984- 416	J131937.25+005043.8	1.005 ± 0.028	8.417 ± 0.032	8.469	–1.352 ± 0.008	–0.966 ± 0.007	2.184 ± 0.005	0.774
11	297- 51959- 442	J132654.62+011346.5	1.175 ± 0.028	8.178 ± 0.026	8.348	–1.434 ± 0.013	–1.041 ± 0.013	2.278 ± 0.011	0.822
12	299- 51671- 311	J133649.51-001158.9	0.977 ± 0.040	8.381 ± 0.045	8.615	–1.222 ± 0.008	–0.911 ± 0.007	1.945 ± 0.005	0.731
13	304- 51957- 12	J142214.30-003919.8	1.411 ± 0.044	7.971 ± 0.028	8.076	–1.580 ± 0.026	–1.126 ± 0.014	2.426 ± 0.024	0.804
14	304- 51957- 568	J142200.19+010213.2	0.994 ± 0.056	8.400 ± 0.057	8.448	–1.225 ± 0.008	–0.812 ± 0.011	1.938 ± 0.006	0.667
15	308- 51662- 412	J144458.53+004618.8	0.972 ± 0.048	8.432 ± 0.054	8.706	–1.009 ± 0.008	–0.887 ± 0.011	1.796 ± 0.007	0.758
16	309- 51994- 489	J145533.67+003657.2	1.126 ± 0.053	8.232 ± 0.039	8.577	–1.006 ± 0.006	–0.727 ± 0.007	1.678 ± 0.004	0.617
17	310- 51990- 136	J150356.83-004200.3	1.059 ± 0.045	8.308 ± 0.043	8.358	–1.300 ± 0.010	–0.866 ± 0.008	2.053 ± 0.008	0.720
18	311- 51665- 8	J151320.62-002551.9	1.119 ± 0.064	8.130 ± 0.054	8.842	–0.871 ± 0.007	–0.918 ± 0.012	1.517 ± 0.005	0.711
19	313- 51673- 638	J152830.72+001740.2	1.185 ± 0.039	8.150 ± 0.032	8.454	–1.385 ± 0.013	–0.906 ± 0.009	2.172 ± 0.010	0.770
20	337- 51997- 593	J125526.06-021333.9	1.560 ± 0.029	7.831 ± 0.026	7.854	–2.040 ± 0.048	–1.497 ± 0.018	2.958 ± 0.044	0.942
21	339- 51692- 437	J130324.17-021046.9	0.982 ± 0.053	8.372 ± 0.056	8.493	–1.141 ± 0.007	–0.741 ± 0.006	1.814 ± 0.005	0.670
22	344- 51693- 321	J155957.38+004741.2	1.305 ± 0.058	8.077 ± 0.041	8.739	–1.375 ± 0.022	–1.115 ± 0.029	2.265 ± 0.020	0.854
23	348- 51671- 297	J163012.60-005408.6	1.157 ± 0.045	8.169 ± 0.034	8.474	–1.149 ± 0.010	–0.776 ± 0.016	1.856 ± 0.008	0.685
24	348- 51671- 331	J163107.20+005324.7	1.175 ± 0.055	8.159 ± 0.042	8.084	–1.357 ± 0.010	–0.813 ± 0.008	2.084 ± 0.009	0.698
25	350- 51691- 500	J171212.07+650248.4	1.137 ± 0.065	8.072 ± 0.049	8.819	–0.786 ± 0.004	–0.773 ± 0.006	1.320 ± 0.002	0.625
26	351- 51780- 212	J170201.44+604746.3	1.003 ± 0.040	8.316 ± 0.038	8.616	–0.963 ± 0.005	–0.739 ± 0.005	1.579 ± 0.003	0.636
27	351- 51780- 600	J170922.63+614851.1	1.046 ± 0.066	8.251 ± 0.058	8.622	–1.029 ± 0.008	–0.705 ± 0.009	1.612 ± 0.006	0.607
28	353- 51703- 479	J170517.74+593546.6	1.127 ± 0.063	8.152 ± 0.047	8.589	–1.036 ± 0.006	–0.669 ± 0.005	1.618 ± 0.005	0.600
29	358- 51818- 403	J173021.82+571531.6	1.074 ± 0.061	8.297 ± 0.055	8.568	–1.181 ± 0.010	–0.848 ± 0.011	1.942 ± 0.008	0.721
30	363- 51989- 532	J153258.27+004100.2	1.036 ± 0.065	8.346 ± 0.062	8.694	–0.837 ± 0.006	–0.729 ± 0.007	1.558 ± 0.003	0.673
31	364- 52000- 66	J163006.89-001810.8	1.106 ± 0.063	8.255 ± 0.053	8.483	–1.162 ± 0.009	–0.789 ± 0.007	1.898 ± 0.007	0.687
32	364- 52000- 384	J162150.66+003509.2	1.337 ± 0.079	8.018 ± 0.041	8.334	–1.048 ± 0.007	-0.576 ± 0.006	1.647 ± 0.005	0.537
33	374- 51791- 612	J221823.86+003918.3	1.097 ± 0.074	8.260 ± 0.065	8.315	–1.214 ± 0.013	–0.780 ± 0.010	1.965 ± 0.011	0.714
34	375- 52140- 118	J222510.13-001152.8	1.413 ± 0.020	7.972 ± 0.020	7.984	–1.763 ± 0.012	–1.250 ± 0.008	2.680 ± 0.010	0.896
35	375- 52140- 348	J221823.86+003918.3	1.150 ± 0.063	8.213 ± 0.051	8.343	–1.213 ± 0.012	–0.787 ± 0.009	1.969 ± 0.009	0.700
36	380- 51792- 253	J225906.70-005810.2	0.972 ± 0.058	8.459 ± 0.065	8.619	–1.131 ± 0.007	–0.931 ± 0.008	1.911 ± 0.005	0.716
37	384- 51821- 281	J232936.56-011057.0	1.184 ± 0.025	8.192 ± 0.024	8.217	–1.384 ± 0.008	–0.931 ± 0.007	2.249 ± 0.006	0.821
38	386- 51788- 573	J235347.69+005402.1	1.194 ± 0.088	8.179 ± 0.067	8.217	–1.379 ± 0.033	–0.866 ± 0.023	2.182 ± 0.031	0.742
39	388- 51793- 239	J000703.98-003447.6	1.246 ± 0.033	8.128 ± 0.027	8.163	–1.468 ± 0.015	–0.970 ± 0.011	2.313 ± 0.013	0.792
40	388- 51793- 457	J000657.02+005125.9	1.221 ± 0.029	8.173 ± 0.025	8.492	–1.345 ± 0.009	–0.989 ± 0.009	2.215 ± 0.006	0.799
41	394- 51913- 402	J005105.28+004600.1	0.982 ± 0.049	8.426 ± 0.051	8.177	–1.297 ± 0.008	–0.814 ± 0.005	2.034 ± 0.007	0.684
42	398- 51789- 223	J011633.94-002043.0	1.144 ± 0.076	8.187 ± 0.063	8.115	–1.281 ± 0.015	–0.750 ± 0.010	2.002 ± 0.013	0.699
43	406- 51869- 484	J022407.68+003226.1	1.141 ± 0.072	8.194 ± 0.053	8.104	–1.309 ± 0.010	–0.699 ± 0.006	1.956 ± 0.008	0.609
44	408- 51821- 472	J023900.79+001836.0	1.265 ± 0.037	8.140 ± 0.033	8.376	–1.509 ± 0.028	–1.145 ± 0.027	2.455 ± 0.026	0.891
45	409- 51871- 50	J024939.72-011151.3	1.309 ± 0.033	8.042 ± 0.028	8.013	–1.652 ± 0.015	–1.060 ± 0.010	2.519 ± 0.013	0.857
46	414- 51901- 546	J032750.16+010135.0	1.057 ± 0.048	8.296 ± 0.038	8.472	–1.104 ± 0.006	–0.689 ± 0.004	1.742 ± 0.004	0.601
47	415- 51810- 285	J033031.22-005846.5	1.178 ± 0.034	8.199 ± 0.031	8.127	–1.481 ± 0.013	–0.972 ± 0.008	2.343 ± 0.010	0.815
48	419- 51879- 364	J004236.94+160202.7	1.103 ± 0.042	8.265 ± 0.040	8.814	–1.091 ± 0.010	–1.054 ± 0.030	1.926 ± 0.008	0.807
49	420- 51871- 156	J005425.68+144852.2	1.156 ± 0.035	8.206 ± 0.029	8.160	–1.406 ± 0.009	–0.929 ± 0.007	2.190 ± 0.007	0.737
50	420- 51871- 474	J005300.53+150129.6	1.200 ± 0.060	8.136 ± 0.042	8.138	–1.282 ± 0.012	–0.748 ± 0.008	1.957 ± 0.009	0.633
51	423- 51821- 402	J011354.58+153947.8	1.265 ± 0.036	8.075 ± 0.027	8.131	–1.426 ± 0.011	–0.955 ± 0.009	2.214 ± 0.008	0.761

Table 1. continued.

(1)	(2)	(3)	(4)	(5)	(6)	(7)	(8)	(9)	(10)
Num	Plate-MJD-FiberID	IAU designations	t_3 (10^4K)	12+log(O/H)$_{T_e}$	(O/H)$_{\rm Bay}$	N2	S 2	O3N2	P
52	424- 51893- 368	J012223.90+152031.9	1.146 ± 0.036	8.226 ± 0.034	8.812	–1.038 ± 0.007	–1.008 ± 0.012	1.897 ± 0.005	0.822
53	430- 51877- 97	J015453.90+130721.7	1.173 ± 0.083	8.190 ± 0.065	8.165	–1.256 ± 0.021	–0.711 ± 0.010	1.971 ± 0.016	0.649
54	431- 51877- 191	J073256.71+370449.8	0.966 ± 0.039	8.372 ± 0.042	8.697	–0.981 ± 0.005	–0.851 ± 0.007	1.640 ± 0.003	0.684
55	436- 51883- 391	J075446.42+451502.7	0.975 ± 0.045	8.348 ± 0.048	8.615	–1.022 ± 0.008	–0.776 ± 0.010	1.677 ± 0.006	0.695
56	442- 51882- 223	J082001.71+505039.1	1.099 ± 0.046	8.265 ± 0.039	8.499	–1.206 ± 0.011	–0.818 ± 0.009	1.941 ± 0.010	0.689
57	443- 51873- 542	J083108.23+493159.1	1.145 ± 0.039	8.177 ± 0.032	8.028	–1.407 ± 0.012	–0.896 ± 0.008	2.147 ± 0.010	0.732
58	446- 51899- 86	J084526.52+531916.2	1.011 ± 0.050	8.658 ± 0.063	8.196	–1.290 ± 0.008	–0.819 ± 0.007	2.010 ± 0.006	0.393
59	446- 51899- 283	J083516.99+533211.0	0.979 ± 0.050	8.409 ± 0.051	8.491	–1.202 ± 0.007	–0.796 ± 0.006	1.881 ± 0.005	0.642
60	446- 51899- 352	J083313.18+542222.8	1.062 ± 0.054	8.305 ± 0.053	8.403	–1.320 ± 0.013	–0.907 ± 0.011	2.106 ± 0.011	0.760
61	446- 51899- 541	J084703.00+545039.4	1.114 ± 0.051	8.231 ± 0.042	8.086	–1.404 ± 0.023	–0.780 ± 0.008	2.123 ± 0.021	0.684
62	447- 51877- 172	J084852.46+514532.7	1.058 ± 0.065	8.328 ± 0.062	8.112	–1.452 ± 0.017	–0.826 ± 0.009	2.212 ± 0.014	0.703
63	452- 51911- 387	J092635.26+582047.4	1.251 ± 0.060	8.123 ± 0.048	8.049	–1.750 ± 0.065	–1.119 ± 0.037	2.651 ± 0.063	0.870
64	452- 51911- 487	J093248.77+582530.7	1.018 ± 0.039	8.324 ± 0.039	8.500	–1.194 ± 0.007	–0.796 ± 0.006	1.883 ± 0.005	0.687
65	454- 51908- 111	J022907.37-085726.2	1.051 ± 0.035	8.318 ± 0.034	8.186	–1.328 ± 0.011	–0.894 ± 0.011	2.104 ± 0.010	0.747
66	455- 51909- 369	J023426.93-072807.6	1.187 ± 0.077	8.163 ± 0.056	8.149	–1.315 ± 0.016	–0.745 ± 0.010	2.015 ± 0.014	0.647
67	456- 51910- 195	J024453.66-082137.8	1.236 ± 0.032	8.101 ± 0.023	8.046	–1.493 ± 0.010	–0.926 ± 0.008	2.260 ± 0.008	0.740
68	458- 51929- 42	J030539.70-083905.4	1.261 ± 0.075	8.142 ± 0.057	8.207	–1.420 ± 0.028	–0.930 ± 0.018	2.312 ± 0.026	0.816
69	458- 51929- 185	J030321.41-075923.2	1.480 ± 0.024	7.898 ± 0.021	7.898	–1.586 ± 0.016	–1.414 ± 0.030	2.482 ± 0.014	0.902
70	459- 51924- 253	J031023.95-083432.8	1.016 ± 0.039	8.377 ± 0.042	8.480	–1.334 ± 0.010	–0.958 ± 0.007	2.137 ± 0.008	0.767
71	460- 51924- 128	J032101.01-080150.1	1.020 ± 0.047	8.333 ± 0.049	8.429	–1.263 ± 0.008	–0.843 ± 0.007	1.985 ± 0.006	0.714
72	460- 51924- 592	J032613.63-063512.4	1.110 ± 0.023	8.269 ± 0.023	8.754	–1.101 ± 0.007	–0.937 ± 0.009	1.939 ± 0.005	0.798
73	463- 51908- 299	J034543.94-065446.0	1.126 ± 0.064	8.215 ± 0.052	8.362	–1.176 ± 0.009	–0.730 ± 0.008	1.853 ± 0.007	0.641
74	467- 51901- 628	J085201.82+010459.5	1.226 ± 0.035	8.104 ± 0.025	8.081	–1.387 ± 0.012	–0.858 ± 0.008	2.136 ± 0.009	0.725
75	468- 51912- 250	J085207.68-001117.8	1.034 ± 0.049	8.344 ± 0.046	8.571	–1.212 ± 0.016	–0.846 ± 0.012	1.941 ± 0.014	0.688
76	469- 51913- 110	J090106.55+005418.0	1.192 ± 0.024	8.183 ± 0.022	8.307	–1.443 ± 0.010	–1.011 ± 0.008	2.306 ± 0.008	0.818
77	472- 51955- 546	J091652.23+003114.1	1.017 ± 0.042	8.344 ± 0.043	8.153	–1.342 ± 0.009	–0.882 ± 0.007	2.087 ± 0.007	0.733
78	474- 52000- 610	J092918.38+002813.0	1.298 ± 0.023	8.071 ± 0.022	8.041	–1.625 ± 0.011	–1.161 ± 0.009	2.532 ± 0.009	0.885
79	483- 51924- 495	J090047.45+574255.0	1.037 ± 0.039	8.322 ± 0.041	8.724	–1.059 ± 0.006	–0.910 ± 0.009	1.826 ± 0.004	0.757
80	483- 51924- 594	J090139.89+575945.9	1.087 ± 0.040	8.271 ± 0.036	8.124	–1.311 ± 0.009	–0.788 ± 0.008	2.047 ± 0.006	0.698
81	489- 51930- 434	J103007.42+654756.0	1.171 ± 0.079	8.164 ± 0.060	8.103	–1.305 ± 0.015	–0.725 ± 0.010	2.005 ± 0.012	0.665
82	490- 51929- 363	J105506.12+670918.3	1.188 ± 0.040	8.150 ± 0.028	8.094	–1.338 ± 0.008	–0.818 ± 0.006	2.053 ± 0.006	0.678
83	490- 51929- 396	J105032.50+661654.1	1.211 ± 0.038	8.152 ± 0.030	8.100	–1.524 ± 0.014	–0.945 ± 0.010	2.353 ± 0.012	0.786
84	493- 51957- 144	J121333.58+665053.8	1.280 ± 0.066	8.064 ± 0.042	8.129	–1.326 ± 0.013	–0.797 ± 0.009	2.022 ± 0.009	0.645
85	493- 51957- 219	J120821.93+661905.8	1.217 ± 0.054	8.138 ± 0.041	8.097	–1.439 ± 0.015	–0.825 ± 0.009	2.222 ± 0.013	0.738
86	502- 51957- 7	J101430.99+004754.9	1.185 ± 0.024	8.142 ± 0.021	8.481	–1.323 ± 0.007	–0.939 ± 0.007	2.112 ± 0.005	0.784
87	505- 52317- 228	J103412.22+014248.9	1.501 ± 0.043	7.858 ± 0.026	7.977	–1.757 ± 0.023	–1.104 ± 0.012	2.577 ± 0.021	0.826
88	507- 52353- 87	J105331.42+011740.5	1.231 ± 0.038	8.130 ± 0.029	8.112	–1.496 ± 0.014	–0.942 ± 0.009	2.305 ± 0.012	0.764
89	507- 52353- 347	J104642.48+022930.1	1.126 ± 0.060	8.212 ± 0.047	8.472	–1.147 ± 0.008	–0.752 ± 0.009	1.804 ± 0.006	0.618
90	509- 52374- 268	J110719.03+015909.6	1.226 ± 0.057	8.199 ± 0.051	8.144	–1.742 ± 0.043	–1.286 ± 0.040	2.724 ± 0.041	0.909
91	509- 52374- 592	J111224.38+022734.5	1.517 ± 0.117	7.903 ± 0.054	8.408	–1.049 ± 0.014	-0.636 ± 0.013	1.737 ± 0.010	0.595
92	512- 51992- 524	J112938.16+031503.9	1.010 ± 0.060	8.359 ± 0.057	8.497	–1.104 ± 0.008	–0.713 ± 0.006	1.730 ± 0.005	0.585
93	513- 51989- 521	J113655.80+033333.4	1.073 ± 0.062	8.257 ± 0.053	8.462	–1.145 ± 0.010	–0.739 ± 0.010	1.797 ± 0.008	0.638
94	515- 52051- 378	J115117.02+032656.0	1.134 ± 0.052	8.237 ± 0.042	8.304	–1.236 ± 0.012	–0.835 ± 0.010	1.992 ± 0.010	0.696
95	516- 52017- 403	J120055.63+032403.9	1.535 ± 0.029	7.841 ± 0.022	7.909	–1.806 ± 0.019	–1.257 ± 0.016	2.691 ± 0.017	0.906
96	519- 52283- 507	J122416.44+030036.0	1.059 ± 0.063	8.286 ± 0.058	8.228	–1.238 ± 0.011	–0.773 ± 0.012	1.923 ± 0.009	0.665
97	519- 52283- 615	J122948.09+030658.6	1.203 ± 0.043	8.112 ± 0.033	8.048	–1.359 ± 0.012	–0.804 ± 0.009	2.103 ± 0.009	0.739
98	524- 52027- 16	J130831.56+012208.0	1.133 ± 0.036	8.228 ± 0.032	8.495	–1.304 ± 0.008	–0.928 ± 0.008	2.103 ± 0.006	0.761
99	524- 52027- 260	J130148.03+013718.4	1.074 ± 0.033	8.319 ± 0.033	8.256	–1.412 ± 0.010	–0.949 ± 0.009	2.239 ± 0.008	0.774
100	525- 52295- 626	J131710.87+025620.0	1.146 ± 0.029	8.218 ± 0.027	8.273	–1.421 ± 0.023	–0.992 ± 0.010	2.258 ± 0.020	0.804
101	527- 52342- 247	J132654.62+011346.9	1.255 ± 0.023	8.108 ± 0.020	8.210	–1.415 ± 0.010	–0.999 ± 0.011	2.273 ± 0.008	0.823
102	530- 52026- 525	J135155.89+032524.2	1.052 ± 0.036	8.264 ± 0.038	8.834	–1.036 ± 0.007	–0.992 ± 0.015	1.787 ± 0.005	0.785
103	535- 51999- 52	J143210.15+012551.9	1.086 ± 0.038	8.243 ± 0.037	8.823	–1.167 ± 0.008	–1.051 ± 0.013	1.939 ± 0.006	0.785
104	539- 52017- 356	J145814.74+020652.2	1.111 ± 0.050	8.240 ± 0.041	8.239	–1.241 ± 0.008	–0.773 ± 0.007	1.950 ± 0.007	0.666

Table 1. continued.

(1)	(2)	(3)	(4)	(5)	(6)	(7)	(8)	(9)	(10)
Num	Plate-MJD-FiberID	IAU designations	t_3 (10^4K)	12+log(O/H)$_{T_e}$	(O/H)$_{Bay}$	N2	S2	O3N2	P
105	544- 52201- 67	J080139.46+382305.2	1.086 ± 0.036	8.258 ± 0.036	8.414	–1.353 ± 0.010	–0.947 ± 0.008	2.141 ± 0.008	0.781
106	544- 52201- 610	J080406.22+393656.8	1.067 ± 0.068	8.209 ± 0.062	8.624	–0.983 ± 0.011	–0.770 ± 0.010	1.610 ± 0.009	0.673
107	548- 51986- 324	J081829.71+453309.3	1.339 ± 0.098	8.011 ± 0.054	8.163	–1.227 ± 0.012	–0.676 ± 0.008	1.855 ± 0.010	0.572
108	548- 51986- 347	J082059.30+461823.4	1.027 ± 0.043	8.314 ± 0.043	8.052	–1.310 ± 0.008	–0.810 ± 0.006	2.026 ± 0.006	0.715
109	549- 51981- 90	J083350.23+454933.6	0.947 ± 0.049	8.453 ± 0.056	8.591	–1.137 ± 0.012	–0.832 ± 0.009	1.855 ± 0.011	0.697
110	550- 51959- 485	J083914.95+481518.3	1.188 ± 0.081	8.130 ± 0.058	8.248	–1.175 ± 0.011	–0.712 ± 0.008	1.801 ± 0.008	0.598
111	553- 51999- 134	J091052.58+522756.5	1.040 ± 0.043	8.335 ± 0.039	8.282	–1.234 ± 0.007	–0.777 ± 0.005	1.915 ± 0.004	0.628
112	555- 52266- 517	J093126.23+551221.6	1.121 ± 0.030	8.244 ± 0.025	8.547	–1.270 ± 0.008	–0.892 ± 0.007	2.045 ± 0.006	0.731
113	557- 52253- 590	J095513.13+573203.1	1.169 ± 0.074	8.152 ± 0.056	8.603	–1.148 ± 0.011	–0.798 ± 0.012	1.842 ± 0.009	0.683
114	560- 52296- 204	J103103.99+585602.0	1.075 ± 0.066	8.199 ± 0.054	8.699	–0.847 ± 0.006	–0.727 ± 0.008	1.381 ± 0.004	0.565
115	564- 52224- 363	J084216.95+033806.7	1.094 ± 0.044	8.298 ± 0.043	8.272	–1.315 ± 0.046	–1.000 ± 0.018	2.178 ± 0.044	0.819
116	566- 52238- 497	J090531.08+033530.4	1.484 ± 0.018	7.871 ± 0.018	7.914	–1.758 ± 0.012	–1.207 ± 0.008	2.632 ± 0.009	0.898
117	568- 52254- 244	J092251.26+025607.4	1.078 ± 0.049	8.277 ± 0.041	8.575	–1.078 ± 0.007	–0.747 ± 0.006	1.765 ± 0.005	0.648
118	569- 52264- 609	J093815.91+043408.4	1.106 ± 0.037	8.245 ± 0.035	8.713	–1.243 ± 0.009	–0.981 ± 0.008	2.054 ± 0.007	0.798
119	570- 52266- 61	J094646.66+033812.8	1.145 ± 0.061	8.220 ± 0.053	8.557	–1.196 ± 0.011	–0.928 ± 0.015	2.016 ± 0.008	0.779
120	582- 52045- 445	J140725.32+052837.9	1.234 ± 0.028	8.103 ± 0.025	8.032	–1.533 ± 0.012	–1.059 ± 0.013	2.373 ± 0.010	0.834
121	587- 52026- 155	J144610.32+033921.6	1.105 ± 0.039	8.228 ± 0.030	8.573	–1.099 ± 0.006	–0.741 ± 0.007	1.773 ± 0.004	0.648
122	587- 52026- 495	J144441.37+040941.7	1.679 ± 0.022	7.841 ± 0.021	7.930	–2.036 ± 0.029	–1.621 ± 0.025	3.052 ± 0.027	0.961
123	588- 52045- 483	J145424.60+035925.0	1.183 ± 0.051	8.177 ± 0.036	8.573	–1.069 ± 0.009	–0.803 ± 0.010	1.799 ± 0.007	0.671
124	589- 52055- 483	J150339.41+035051.7	1.159 ± 0.078	8.138 ± 0.062	8.574	–1.051 ± 0.010	–0.764 ± 0.009	1.728 ± 0.007	0.682
125	590- 52057- 200	J151045.41+033038.5	1.094 ± 0.057	8.272 ± 0.049	8.213	–1.231 ± 0.010	–0.748 ± 0.007	1.925 ± 0.006	0.635
126	594- 52045- 493	J154654.55+030902.1	1.154 ± 0.025	8.209 ± 0.022	8.554	–1.327 ± 0.009	–0.971 ± 0.007	2.150 ± 0.007	0.788
127	597- 52059- 460	J113303.79+651341.1	1.363 ± 0.053	8.012 ± 0.035	8.193	–1.420 ± 0.032	–1.098 ± 0.041	2.292 ± 0.030	0.842
128	597- 52059- 586	J114047.42+644710.3	1.102 ± 0.032	8.274 ± 0.029	8.313	–1.345 ± 0.008	–0.920 ± 0.007	2.133 ± 0.006	0.735
129	602- 52072- 19	J131426.57+633311.5	1.057 ± 0.052	8.302 ± 0.048	8.595	–1.142 ± 0.007	–0.833 ± 0.007	1.854 ± 0.005	0.681
130	605- 52353- 616	J141145.34+623911.1	1.106 ± 0.052	8.269 ± 0.048	8.508	–1.258 ± 0.016	–0.921 ± 0.029	2.081 ± 0.014	0.786
131	606- 52365- 604	J142619.15+622750.0	1.048 ± 0.039	8.328 ± 0.039	8.559	–1.329 ± 0.010	–0.972 ± 0.008	2.128 ± 0.008	0.771
132	608- 52081- 255	J144329.11+585543.6	1.195 ± 0.084	8.116 ± 0.064	8.043	–1.375 ± 0.014	–0.816 ± 0.010	2.079 ± 0.011	0.695
133	609- 52339- 441	J144845.84+634620.2	1.062 ± 0.054	8.323 ± 0.053	8.203	–1.346 ± 0.012	–0.874 ± 0.019	2.145 ± 0.010	0.752
134	613- 52345- 342	J150728.68+595913.2	1.138 ± 0.034	8.164 ± 0.028	8.759	–1.039 ± 0.006	–0.909 ± 0.008	1.773 ± 0.004	0.753
135	615- 52347- 606	J153737.27+584740.5	1.253 ± 0.053	8.124 ± 0.041	8.542	–1.147 ± 0.046	–1.027 ± 0.023	2.023 ± 0.045	0.833
136	616- 52374- 349	J153534.13+545534.3	1.102 ± 0.037	8.269 ± 0.032	8.613	–1.132 ± 0.007	–0.891 ± 0.011	1.906 ± 0.005	0.727
137	620- 52375- 428	J155829.49+520650.7	1.032 ± 0.061	8.285 ± 0.057	8.621	–1.031 ± 0.007	–0.778 ± 0.008	1.659 ± 0.005	0.637
138	620- 52375- 506	J160041.62+514443.0	1.230 ± 0.060	8.132 ± 0.047	8.118	–1.319 ± 0.017	–0.742 ± 0.009	2.075 ± 0.008	0.696
139	621- 52055- 618	J161156.30+532630.1	1.064 ± 0.047	8.305 ± 0.041	8.144	–1.275 ± 0.010	–0.745 ± 0.007	1.970 ± 0.008	0.642
140	623- 52051- 396	J161031.34+522305.9	1.405 ± 0.057	7.905 ± 0.037	7.929	–1.628 ± 0.025	–1.058 ± 0.016	2.426 ± 0.023	0.833
141	625- 52145- 72	J163106.19+484527.0	1.812 ± 0.177	7.664 ± 0.058	8.148	–1.216 ± 0.017	–0.632 ± 0.012	1.810 ± 0.013	0.550
142	627- 52144- 253	J163240.72+463338.1	0.986 ± 0.054	8.365 ± 0.056	8.681	–0.977 ± 0.006	–0.823 ± 0.009	1.665 ± 0.005	0.697
143	627- 52144- 295	J163055.78+461805.7	1.052 ± 0.050	8.329 ± 0.050	8.566	–1.184 ± 0.010	–0.895 ± 0.014	1.976 ± 0.009	0.753
144	627- 52144- 446	J163445.34+465903.1	1.010 ± 0.040	8.372 ± 0.043	8.534	–1.212 ± 0.011	–0.853 ± 0.009	1.980 ± 0.009	0.741
145	628- 52083- 555	J164235.52+422349.5	1.105 ± 0.031	8.232 ± 0.026	8.589	–1.164 ± 0.006	–0.857 ± 0.007	1.893 ± 0.004	0.707
146	629- 52051- 497	J164359.16+443632.7	0.957 ± 0.045	8.473 ± 0.051	8.481	–1.260 ± 0.008	–0.872 ± 0.007	2.002 ± 0.006	0.678
147	631- 52079- 307	J164645.10+413208.8	1.242 ± 0.091	8.064 ± 0.066	8.023	–1.430 ± 0.019	–0.826 ± 0.013	2.154 ± 0.016	0.725
148	633- 52079- 336	J165711.23+401915.6	1.080 ± 0.064	8.273 ± 0.061	8.291	–1.249 ± 0.011	–0.829 ± 0.009	2.032 ± 0.009	0.765
149	636- 52176- 439	J205430.86-061739.8	1.217 ± 0.089	8.116 ± 0.062	8.300	–1.142 ± 0.012	–0.706 ± 0.008	1.831 ± 0.010	0.650
150	637- 52174- 399	J210114.40-055510.2	1.056 ± 0.029	8.360 ± 0.029	8.401	–1.333 ± 0.011	–0.905 ± 0.008	2.165 ± 0.010	0.759
151	639- 52146- 143	J211902.28-074226.6	1.276 ± 0.047	8.048 ± 0.033	8.032	–1.447 ± 0.011	–0.907 ± 0.010	2.210 ± 0.009	0.753
152	648- 52559- 288	J234148.29-105619.6	1.049 ± 0.048	8.279 ± 0.045	8.163	–1.223 ± 0.008	–0.754 ± 0.006	1.905 ± 0.006	0.681
153	649- 52201- 637	J235604.68-085423.4	1.121 ± 0.044	8.233 ± 0.040	8.120	–1.427 ± 0.016	–0.933 ± 0.014	2.227 ± 0.014	0.778
154	651- 52141- 304	J000430.34-101129.7	1.489 ± 0.055	7.865 ± 0.033	7.933	–1.594 ± 0.034	–1.322 ± 0.047	2.434 ± 0.033	0.856
155	656- 52148- 140	J004645.72-105410.4	1.128 ± 0.072	8.283 ± 0.063	8.290	–1.346 ± 0.015	–0.886 ± 0.011	2.196 ± 0.012	0.765
156	658- 52146- 17	J010513.49-103740.8	1.187 ± 0.041	8.202 ± 0.035	8.136	–1.529 ± 0.014	–0.978 ± 0.009	2.377 ± 0.012	0.780
157	659- 52199- 307	J010409.91-095346.6	1.205 ± 0.074	8.129 ± 0.055	8.060	–1.486 ± 0.019	–0.830 ± 0.011	2.218 ± 0.017	0.701

Table 1. continued.

(1)	(2)	(3)	(4)	(5)	(6)	(7)	(8)	(9)	(10)
Num	Plate-MJD-FiberID	IAU designations	t_3 (10^4K)	12+log(O/H)$_{T_e}$	(O/H)$_{\rm Bay}$	N2	S2	O3N2	P
158	659- 52199- 435	J010643.32-092223.1	1.117 ± 0.059	8.255 ± 0.054	8.159	–1.369 ± 0.016	–0.871 ± 0.012	2.171 ± 0.012	0.755
159	660- 52177- 414	J011616.82-085021.4	1.263 ± 0.041	8.060 ± 0.029	8.070	–1.386 ± 0.011	–0.900 ± 0.008	2.154 ± 0.009	0.756
160	660- 52177- 450	J011729.09-084403.8	1.045 ± 0.038	8.305 ± 0.036	8.567	–1.139 ± 0.008	–0.824 ± 0.009	1.855 ± 0.005	0.697
161	663- 52145- 406	J013844.90-083540.5	1.233 ± 0.046	8.118 ± 0.033	8.114	–1.404 ± 0.013	–0.860 ± 0.009	2.184 ± 0.011	0.738
162	664- 52174- 112	J014721.67-091646.2	1.139 ± 0.042	8.218 ± 0.036	8.123	–1.391 ± 0.016	–0.841 ± 0.013	2.177 ± 0.014	0.750
163	664- 52174- 447	J014713.82-080702.6	1.251 ± 0.063	8.056 ± 0.043	8.038	–1.388 ± 0.014	–0.797 ± 0.009	2.079 ± 0.011	0.682
164	666- 52149- 532	J020356.90-080758.4	1.027 ± 0.048	8.307 ± 0.043	8.594	–1.091 ± 0.007	–0.759 ± 0.007	1.748 ± 0.006	0.653
165	668- 52162- 89	J022037.66-092907.4	1.220 ± 0.028	8.140 ± 0.023	8.407	–1.144 ± 0.006	–0.985 ± 0.007	1.973 ± 0.005	0.793
166	716- 52203- 368	J215637.75-070007.9	1.198 ± 0.082	8.110 ± 0.058	8.352	–1.138 ± 0.009	–0.710 ± 0.008	1.732 ± 0.007	0.574
167	726- 52226- 532	J231322.68-084503.9	1.080 ± 0.068	8.274 ± 0.056	8.484	–1.081 ± 0.008	–0.686 ± 0.007	1.706 ± 0.006	0.576
168	730- 52466- 376	J212442.05+114751.0	1.014 ± 0.037	8.324 ± 0.036	8.610	–1.007 ± 0.005	–0.816 ± 0.005	1.687 ± 0.003	0.682
169	735- 52519- 461	J220802.88+131334.6	1.192 ± 0.041	8.127 ± 0.033	8.485	–1.295 ± 0.009	–0.908 ± 0.008	2.064 ± 0.007	0.768
170	740- 52263- 267	J224422.71+131608.7	1.021 ± 0.063	8.338 ± 0.062	8.544	–1.150 ± 0.010	–0.776 ± 0.007	1.846 ± 0.008	0.673
171	753- 52233- 593	J002652.08+152737.8	1.273 ± 0.066	8.048 ± 0.049	8.722	–1.249 ± 0.031	–1.026 ± 0.027	2.081 ± 0.028	0.845
172	755- 52235- 300	J073928.39+314502.1	1.086 ± 0.039	8.264 ± 0.037	8.063	–1.367 ± 0.009	–0.810 ± 0.006	2.130 ± 0.007	0.743
173	756- 52577- 37	J075507.92+340827.6	1.146 ± 0.035	8.185 ± 0.030	8.729	–1.012 ± 0.006	–0.876 ± 0.009	1.778 ± 0.005	0.758
174	761- 52266- 443	J082542.86+422758.6	1.342 ± 0.025	8.032 ± 0.018	8.117	–1.506 ± 0.011	–0.945 ± 0.012	2.339 ± 0.009	0.788
175	761- 52266- 454	J082614.16+422833.6	1.123 ± 0.074	8.241 ± 0.057	8.431	–1.097 ± 0.009	–0.694 ± 0.007	1.725 ± 0.007	0.560
176	762- 52232- 217	J083343.87+431951.6	1.002 ± 0.058	8.363 ± 0.056	8.157	–1.207 ± 0.008	–0.705 ± 0.007	1.852 ± 0.006	0.614
177	762- 52232- 575	J083803.72+445900.2	1.205 ± 0.050	8.099 ± 0.036	8.598	–1.186 ± 0.011	–0.821 ± 0.010	1.876 ± 0.009	0.689
178	767- 52252- 463	J092429.86+514301.2	1.208 ± 0.048	8.117 ± 0.032	8.124	–1.284 ± 0.009	–0.740 ± 0.006	1.960 ± 0.007	0.644
179	768- 52281- 193	J093733.77+523924.8	1.114 ± 0.068	8.237 ± 0.054	8.290	–1.197 ± 0.009	–0.743 ± 0.007	1.851 ± 0.007	0.603
180	769- 52282- 100	J095131.78+525936.2	1.268 ± 0.021	8.087 ± 0.021	8.027	–1.599 ± 0.009	–1.103 ± 0.006	2.468 ± 0.007	0.849
181	769- 52282- 575	J095408.42+544606.9	1.069 ± 0.040	8.318 ± 0.037	8.366	–1.247 ± 0.034	–0.874 ± 0.009	2.023 ± 0.032	0.719
182	771- 52370- 490	J101242.98+613302.8	1.123 ± 0.030	8.248 ± 0.028	8.105	–1.453 ± 0.009	–0.914 ± 0.007	2.257 ± 0.007	0.757
183	772- 52375- 270	J102132.50+614404.5	1.277 ± 0.067	8.086 ± 0.045	8.303	–1.263 ± 0.014	–0.872 ± 0.012	2.031 ± 0.011	0.709
184	773- 52376- 143	J104500.96+621527.3	1.269 ± 0.083	8.058 ± 0.048	8.594	–0.691 ± 0.005	–0.477 ± 0.006	1.218 ± 0.003	0.491
185	775- 52295- 291	J111439.19+605418.3	1.163 ± 0.039	8.199 ± 0.030	8.311	–1.284 ± 0.009	–0.850 ± 0.007	2.034 ± 0.007	0.693
186	779- 52342- 355	J120725.66+623458.0	0.993 ± 0.043	8.310 ± 0.043	8.709	–0.970 ± 0.006	–0.830 ± 0.006	1.579 ± 0.003	0.652
187	782- 52320- 22	J130445.62+622420.8	0.961 ± 0.042	8.382 ± 0.045	8.695	–0.936 ± 0.005	–0.813 ± 0.005	1.580 ± 0.003	0.663
188	784- 52327- 179	J132002.90+614627.4	1.247 ± 0.088	8.109 ± 0.059	8.196	–1.247 ± 0.015	–0.769 ± 0.011	1.937 ± 0.012	0.624
189	792- 52353- 110	J150127.22+553126.3	1.113 ± 0.072	8.255 ± 0.059	8.160	–1.284 ± 0.012	–0.741 ± 0.009	1.952 ± 0.009	0.601
190	794- 52376- 460	J152045.65+533807.0	1.070 ± 0.054	8.326 ± 0.054	8.421	–1.246 ± 0.019	–0.887 ± 0.015	2.072 ± 0.015	0.770
191	817- 52381- 424	J163210.01+412055.6	1.105 ± 0.043	8.226 ± 0.036	8.487	–1.164 ± 0.009	–0.771 ± 0.009	1.856 ± 0.006	0.672
192	828- 52317- 319	J083145.67+384756.7	1.107 ± 0.067	8.257 ± 0.059	8.188	–1.310 ± 0.014	–0.846 ± 0.013	2.074 ± 0.011	0.718
193	834- 52316- 157	J093855.90+471228.8	1.100 ± 0.053	8.259 ± 0.047	8.096	–1.384 ± 0.011	–0.810 ± 0.008	2.121 ± 0.009	0.695
194	836- 52376- 378	J112145.51+055756.5	1.066 ± 0.039	8.300 ± 0.042	8.537	–1.298 ± 0.010	–0.934 ± 0.011	2.129 ± 0.008	0.821
195	838- 52378- 595	J114359.54+052154.7	1.459 ± 0.033	7.881 ± 0.024	8.717	–1.457 ± 0.014	–1.172 ± 0.013	2.288 ± 0.011	0.854
196	841- 52375- 333	J115641.37+054315.6	1.082 ± 0.067	8.251 ± 0.059	8.567	–1.120 ± 0.009	–0.755 ± 0.008	1.793 ± 0.007	0.655
197	845- 52381- 1	J123523.86+034536.0	1.099 ± 0.049	8.255 ± 0.044	8.159	–1.332 ± 0.011	–0.828 ± 0.018	2.094 ± 0.008	0.732
198	846- 52407- 267	J123538.74+041245.0	1.113 ± 0.041	8.260 ± 0.034	8.420	–1.246 ± 0.007	–0.826 ± 0.006	1.997 ± 0.005	0.691
199	847- 52426- 522	J124954.84+060610.4	1.105 ± 0.035	8.230 ± 0.029	8.338	–1.233 ± 0.007	–0.799 ± 0.006	1.932 ± 0.005	0.676
200	848- 52669- 528	J125657.58+055616.4	0.949 ± 0.055	8.368 ± 0.059	8.678	–0.972 ± 0.006	–0.790 ± 0.007	1.542 ± 0.003	0.611
201	853- 52374- 577	J133810.13+053504.5	1.000 ± 0.055	8.332 ± 0.054	8.672	–1.030 ± 0.006	–0.819 ± 0.006	1.640 ± 0.004	0.616
202	857- 52314- 386	J074034.66+244136.6	1.096 ± 0.038	8.277 ± 0.035	8.366	–1.312 ± 0.029	–0.944 ± 0.012	2.117 ± 0.027	0.763
203	859- 52317- 70	J080000.70+274641.8	1.117 ± 0.031	8.269 ± 0.030	8.189	–1.408 ± 0.009	–0.939 ± 0.007	2.245 ± 0.006	0.781
204	864- 52320- 379	J083833.53+374216.5	1.137 ± 0.064	8.239 ± 0.059	8.416	–1.415 ± 0.034	–1.141 ± 0.039	2.306 ± 0.032	0.862
205	870- 52325- 321	J092600.41+442736.0	1.268 ± 0.029	8.094 ± 0.023	8.459	–1.409 ± 0.011	–1.020 ± 0.011	2.257 ± 0.009	0.813
206	879- 52365- 14	J113247.69+510215.3	1.260 ± 0.046	8.087 ± 0.034	8.724	–1.305 ± 0.016	–1.047 ± 0.010	2.116 ± 0.014	0.785
207	881- 52368- 567	J115240.85+533228.3	0.997 ± 0.049	8.303 ± 0.051	8.603	–0.986 ± 0.006	–0.737 ± 0.006	1.627 ± 0.004	0.692
208	884- 52374- 404	J122611.16+532602.0	1.497 ± 0.027	7.853 ± 0.022	7.937	–1.858 ± 0.019	–1.138 ± 0.009	2.696 ± 0.015	0.861
209	886- 52381- 129	J125427.22+510436.1	1.197 ± 0.083	8.153 ± 0.061	8.184	–1.267 ± 0.013	–0.779 ± 0.010	1.982 ± 0.010	0.661
210	886- 52381- 605	J125931.51+531554.0	1.044 ± 0.049	8.305 ± 0.046	8.601	–1.092 ± 0.008	–0.815 ± 0.008	1.787 ± 0.006	0.678

Table 1. continued.

(1)	(2)	(3)	(4)	(5)	(6)	(7)	(8)	(9)	(10)
Num	Plate-MJD-FiberID	IAU designations	t_3 (10^4K)	12+log(O/H)$_{T_e}$	(O/H)$_{Bay}$	N2	S2	O3N2	P
211	890- 52583- 49	J075308.57+304512.6	1.039 ± 0.044	8.356 ± 0.045	8.227	–1.299 ± 0.010	–0.839 ± 0.009	2.093 ± 0.008	0.742
212	890- 52583- 65	J075454.69+312821.0	1.057 ± 0.063	8.332 ± 0.063	8.336	–1.352 ± 0.016	–0.943 ± 0.011	2.178 ± 0.014	0.783
213	893- 52589- 76	J082010.56+374354.4	1.366 ± 0.081	8.022 ± 0.046	8.171	–1.315 ± 0.016	–0.764 ± 0.010	2.055 ± 0.014	0.657
214	893- 52589- 177	J081755.35+372959.6	1.137 ± 0.066	8.170 ± 0.048	8.501	–1.073 ± 0.007	–0.676 ± 0.006	1.626 ± 0.004	0.541
215	896- 52592- 125	J084419.08+414310.2	1.063 ± 0.039	8.256 ± 0.035	8.714	–0.925 ± 0.005	–0.832 ± 0.007	1.614 ± 0.003	0.696
216	901- 52641- 536	J093816.85+504200.0	1.253 ± 0.038	8.101 ± 0.027	8.260	–1.341 ± 0.015	–0.903 ± 0.013	2.124 ± 0.012	0.736
217	902- 52409- 135	J094903.36+500126.0	1.091 ± 0.037	8.256 ± 0.034	8.608	–1.058 ± 0.006	–0.844 ± 0.008	1.816 ± 0.004	0.743
218	903- 52400- 600	J100751.67+525624.0	1.216 ± 0.050	8.105 ± 0.034	8.076	–1.396 ± 0.017	–0.802 ± 0.008	2.070 ± 0.014	0.648
219	904- 52381- 501	J102024.05+540043.9	1.078 ± 0.044	8.272 ± 0.045	8.162	–1.374 ± 0.011	–0.907 ± 0.009	2.162 ± 0.008	0.780
220	908- 52373- 27	J111558.18+554806.4	1.175 ± 0.037	8.166 ± 0.028	8.334	–1.237 ± 0.007	–0.800 ± 0.006	1.946 ± 0.004	0.667
221	909- 52379- 616	J112313.30+570327.7	1.362 ± 0.027	7.966 ± 0.021	8.004	–1.747 ± 0.022	–1.072 ± 0.010	2.562 ± 0.020	0.823
222	915- 52443- 598	J140539.17-015334.4	1.160 ± 0.068	8.192 ± 0.054	8.146	–1.312 ± 0.011	–0.818 ± 0.008	2.058 ± 0.007	0.699
223	926- 52413- 279	J153804.80-014940.8	1.072 ± 0.063	8.320 ± 0.060	8.352	–1.294 ± 0.008	–0.860 ± 0.007	2.074 ± 0.006	0.716
224	927- 52577- 514	J074553.04+231017.0	1.080 ± 0.048	8.248 ± 0.041	8.681	–0.981 ± 0.007	–0.838 ± 0.011	1.669 ± 0.006	0.681
225	934- 52672- 483	J084725.06+355451.4	1.069 ± 0.025	8.326 ± 0.025	8.570	–1.248 ± 0.008	–0.923 ± 0.008	2.071 ± 0.006	0.771
226	936- 52705- 477	J085949.13+380632.0	1.260 ± 0.032	8.113 ± 0.027	8.118	–1.512 ± 0.014	–0.988 ± 0.010	2.384 ± 0.012	0.830
227	937- 52707- 275	J090741.52+385202.2	1.107 ± 0.066	8.212 ± 0.055	8.610	–1.141 ± 0.009	–0.797 ± 0.009	1.809 ± 0.006	0.659
228	940- 52670- 594	J094330.67+422142.8	1.013 ± 0.058	8.367 ± 0.059	8.429	–1.116 ± 0.009	–0.730 ± 0.008	1.836 ± 0.007	0.680
229	945- 52652- 423	J095859.35+552415.8	1.161 ± 0.040	8.184 ± 0.033	8.214	–1.266 ± 0.010	–0.808 ± 0.007	2.046 ± 0.008	0.752
230	949- 52427- 359	J104337.66+580820.7	1.235 ± 0.040	8.322 ± 0.076	8.049	–1.497 ± 0.013	–0.996 ± 0.010	2.291 ± 0.011	0.523
231	952- 52409- 264	J112509.46+584700.9	1.004 ± 0.046	8.360 ± 0.046	8.612	–1.153 ± 0.007	–0.839 ± 0.006	1.842 ± 0.004	0.667
232	952- 52409- 439	J112555.10+593319.0	1.235 ± 0.025	8.157 ± 0.016	8.197	–1.347 ± 0.009	–0.817 ± 0.006	2.133 ± 0.007	0.695
233	952- 52409- 447	J113116.49+601229.5	1.105 ± 0.058	8.224 ± 0.053	8.103	–1.343 ± 0.013	–0.871 ± 0.011	2.098 ± 0.011	0.753
234	955- 52409- 383	J121142.86+603626.6	1.166 ± 0.054	8.204 ± 0.045	8.235	–1.295 ± 0.013	–0.823 ± 0.012	2.121 ± 0.011	0.779
235	956- 52401- 20	J124340.29+590311.1	1.071 ± 0.070	8.309 ± 0.063	8.258	–1.234 ± 0.015	–0.759 ± 0.009	1.950 ± 0.013	0.652
236	956- 52401- 347	J122630.60+595712.6	1.126 ± 0.063	8.235 ± 0.057	8.144	–1.429 ± 0.024	–0.930 ± 0.013	2.240 ± 0.022	0.778
237	957- 52398- 210	J125328.61+584021.7	1.114 ± 0.027	8.272 ± 0.027	8.306	–1.375 ± 0.009	–0.930 ± 0.007	2.211 ± 0.006	0.785
238	957- 52398- 530	J125856.26+604730.8	1.074 ± 0.045	8.289 ± 0.044	8.297	–1.319 ± 0.012	–0.889 ± 0.009	2.105 ± 0.009	0.759
239	959- 52411- 137	J132455.03+574510.7	1.163 ± 0.028	8.219 ± 0.028	8.760	–1.281 ± 0.009	–1.056 ± 0.010	2.152 ± 0.007	0.824
240	963- 52643- 165	J105315.89+471517.2	1.289 ± 0.057	8.083 ± 0.034	8.472	–1.127 ± 0.009	–0.748 ± 0.008	1.815 ± 0.006	0.608
241	964- 52646- 570	J110918.05+494753.8	1.109 ± 0.030	8.249 ± 0.025	8.453	–1.169 ± 0.007	–0.780 ± 0.006	1.890 ± 0.005	0.674
242	969- 52442- 354	J115630.62+500822.2	1.156 ± 0.036	8.147 ± 0.029	8.764	–1.040 ± 0.007	–0.950 ± 0.013	1.772 ± 0.005	0.748
243	971- 52644- 599	J123153.64+500056.5	1.105 ± 0.057	8.192 ± 0.048	8.673	–1.000 ± 0.007	–0.824 ± 0.010	1.664 ± 0.004	0.680
244	972- 52435- 370	J165844.50+351923.1	1.108 ± 0.035	8.251 ± 0.030	8.329	–1.248 ± 0.008	–0.822 ± 0.007	2.011 ± 0.006	0.724
245	978- 52441- 408	J171400.93+313023.4	1.053 ± 0.043	8.309 ± 0.039	8.621	–1.032 ± 0.007	–0.841 ± 0.013	1.746 ± 0.006	0.681
246	979- 52427- 83	J172006.75+255827.4	1.110 ± 0.066	8.223 ± 0.054	8.219	–1.214 ± 0.014	-0.760 ± 0.010	1.903 ± 0.012	0.664
247	984- 52442- 263	J205510.41-001903.0	1.063 ± 0.065	8.235 ± 0.053	8.740	–0.812 ± 0.005	–0.709 ± 0.006	1.354 ± 0.004	0.558
248	987- 52523- 394	J211958.32+005233.6	1.145 ± 0.039	8.235 ± 0.037	8.138	–1.449 ± 0.012	–0.947 ± 0.009	2.303 ± 0.010	0.806
249	987- 52523- 440	J212043.97+010006.8	1.025 ± 0.058	8.335 ± 0.055	8.513	–1.064 ± 0.007	–0.722 ± 0.006	1.722 ± 0.002	0.624
250	988- 52520- 456	J212829.71+003021.9	1.100 ± 0.067	8.229 ± 0.053	8.274	–1.139 ± 0.009	–0.664 ± 0.007	1.753 ± 0.006	0.588
251	992- 52644- 19	J093625.35+050332.0	1.362 ± 0.036	8.015 ± 0.028	8.118	–1.516 ± 0.013	–1.050 ± 0.014	2.396 ± 0.011	0.844
252	997- 52734- 474	J101637.77+065214.5	1.184 ± 0.079	8.140 ± 0.060	8.078	–1.375 ± 0.017	–0.793 ± 0.011	2.069 ± 0.014	0.668
253	999- 52636- 150	J103404.17+061210.4	1.156 ± 0.036	8.185 ± 0.030	8.587	–1.217 ± 0.008	–0.911 ± 0.007	1.991 ± 0.006	0.754
254	1001- 52670- 385	J104727.84+072238.2	0.983 ± 0.055	8.342 ± 0.060	8.847	–0.909 ± 0.007	–0.919 ± 0.016	1.587 ± 0.005	0.717
255	1001- 52670- 611	J105445.74+073731.8	1.127 ± 0.058	8.230 ± 0.047	8.479	–1.173 ± 0.037	–0.836 ± 0.014	1.897 ± 0.035	0.677
256	1002- 52646- 525	J105854.79+080043.9	0.917 ± 0.051	8.503 ± 0.064	8.578	–1.198 ± 0.008	–0.851 ± 0.008	1.931 ± 0.006	0.711
257	1005- 52703- 268	J094422.13+480130.3	1.446 ± 0.045	7.958 ± 0.033	8.055	–1.813 ± 0.027	–1.169 ± 0.016	2.721 ± 0.023	0.866
258	1007- 52706- 225	J100912.50+500604.6	1.339 ± 0.108	7.910 ± 0.063	8.660	–0.946 ± 0.009	–0.746 ± 0.010	1.532 ± 0.006	0.636
259	1008- 52707- 430	J101855.46+515527.8	1.267 ± 0.033	8.097 ± 0.024	8.153	–1.418 ± 0.011	-0.932 ± 0.012	2.232 ± 0.009	0.765
260	1013- 52707- 229	J111824.48+540115.9	1.188 ± 0.086	8.226 ± 0.071	8.166	–1.562 ± 0.027	–1.002 ± 0.019	2.439 ± 0.024	0.785
261	1014- 52707- 393	J112544.09+550532.2	1.039 ± 0.066	8.275 ± 0.062	8.688	–0.990 ± 0.007	–0.815 ± 0.008	1.631 ± 0.005	0.656
262	1020- 52721- 287	J122842.45+535723.0	1.183 ± 0.052	8.166 ± 0.047	8.131	–1.455 ± 0.014	–0.965 ± 0.011	2.308 ± 0.012	0.842
263	1021- 52460- 446	J204018.05+010324.4	1.075 ± 0.064	8.253 ± 0.058	8.536	–1.156 ± 0.009	–0.782 ± 0.007	1.871 ± 0.007	0.714

Table 1. continued.

(1)	(2)	(3)	(4)	(5)	(6)	(7)	(8)	(9)	(10)
Num	Plate-MJD-FiberID	IAU designations	t_3 (10^4K)	12+log(O/H)$_{T_e}$	(O/H)$_{\rm Bay}$	N2	S2	O3N2	P
264	1024- 52826- 106	J210134.44-002846.9	1.401 ± 0.099	7.982 ± 0.056	8.150	–1.370 ± 0.027	–0.824 ± 0.024	2.159 ± 0.025	0.726
265	1026- 52558- 122	J211451.48-011046.2	1.142 ± 0.062	8.210 ± 0.051	8.109	–1.378 ± 0.018	–0.823 ± 0.009	2.133 ± 0.016	0.714
266	1026- 52558- 596	J211829.85+003059.4	1.262 ± 0.041	8.102 ± 0.029	8.395	–1.320 ± 0.017	–0.904 ± 0.013	2.136 ± 0.015	0.771
267	1028- 52562- 373	J212705.80+005827.1	1.362 ± 0.041	8.011 ± 0.027	8.079	–1.647 ± 0.023	–0.993 ± 0.011	2.475 ± 0.021	0.781
268	1028- 52562- 388	J212702.90+002701.8	1.011 ± 0.056	8.357 ± 0.059	8.464	–1.256 ± 0.012	–0.872 ± 0.009	2.002 ± 0.010	0.728
269	1028- 52562- 422	J212829.71+003021.9	1.004 ± 0.061	8.351 ± 0.058	8.187	–1.139 ± 0.008	–0.645 ± 0.006	1.757 ± 0.006	0.593
270	1028- 52562- 592	J213338.95+002605.2	1.334 ± 0.038	8.024 ± 0.025	8.074	–1.610 ± 0.018	–0.961 ± 0.009	2.409 ± 0.015	0.758
271	1028- 52884- 386	J212705.80+005827.1	1.291 ± 0.040	8.071 ± 0.028	8.125	–1.552 ± 0.020	–0.951 ± 0.010	2.368 ± 0.018	0.772
272	1028- 52884- 562	J213338.95+002605.2	1.328 ± 0.032	8.029 ± 0.022	8.084	–1.597 ± 0.015	–0.962 ± 0.008	2.409 ± 0.012	0.776
273	1030- 52914- 77	J214642.29+000009.0	1.076 ± 0.047	8.498 ± 0.057	8.227	–1.420 ± 0.010	–0.957 ± 0.009	2.248 ± 0.008	0.562
274	1030- 52914- 107	J214459.59-001140.2	1.003 ± 0.050	8.355 ± 0.051	8.441	–1.242 ± 0.009	–0.829 ± 0.006	1.946 ± 0.007	0.693
275	1032- 53175- 635	J220412.46+002201.5	1.328 ± 0.058	8.045 ± 0.045	8.058	–1.512 ± 0.019	–0.862 ± 0.011	2.356 ± 0.012	0.795
276	1033- 52822- 458	J220707.90+004658.8	1.306 ± 0.097	8.035 ± 0.064	8.102	–1.473 ± 0.031	–0.865 ± 0.015	2.269 ± 0.029	0.773
277	1034- 52525- 551	J221549.25+010938.8	1.197 ± 0.053	8.141 ± 0.040	8.110	–1.341 ± 0.014	–0.818 ± 0.008	2.092 ± 0.012	0.722
278	1034- 52813- 521	J221549.25+010938.8	1.091 ± 0.047	8.273 ± 0.041	8.095	–1.372 ± 0.011	–0.816 ± 0.006	2.123 ± 0.009	0.706
279	1035- 52816- 574	J222358.95+005007.8	1.217 ± 0.037	8.170 ± 0.032	8.301	–1.310 ± 0.046	–1.008 ± 0.012	2.202 ± 0.044	0.840
280	1040- 52722- 21	J132150.45+534127.9	1.221 ± 0.061	8.127 ± 0.047	8.083	–1.545 ± 0.016	–0.908 ± 0.011	2.335 ± 0.014	0.755
281	1040- 52722- 358	J130728.44+542652.4	1.123 ± 0.061	8.204 ± 0.045	8.166	–1.172 ± 0.007	–0.702 ± 0.006	1.702 ± 0.001	0.501
282	1042- 52725- 399	J133446.30+534927.4	1.172 ± 0.052	8.162 ± 0.046	8.768	–1.319 ± 0.017	–1.098 ± 0.030	2.146 ± 0.015	0.827
283	1043- 52465- 78	J135624.07+523851.0	1.203 ± 0.077	8.095 ± 0.058	8.613	–1.191 ± 0.013	–0.880 ± 0.014	1.896 ± 0.011	0.712
284	1052- 52466- 115	J153808.50+431421.1	1.164 ± 0.078	8.174 ± 0.057	8.530	–1.067 ± 0.009	–0.684 ± 0.007	1.708 ± 0.006	0.595
285	1054- 52516- 499	J155411.09+400602.8	1.098 ± 0.067	8.207 ± 0.061	8.058	–1.299 ± 0.012	–0.769 ± 0.009	2.001 ± 0.009	0.718
286	1060- 52636- 21	J075638.45+291819.8	1.342 ± 0.090	7.944 ± 0.048	8.690	–0.834 ± 0.007	–0.731 ± 0.014	1.386 ± 0.005	0.557
287	1060- 52636- 328	J075230.29+301607.6	1.247 ± 0.046	8.076 ± 0.035	8.037	–1.556 ± 0.031	–0.943 ± 0.013	2.341 ± 0.028	0.778
288	1063- 52591- 389	J033128.49+003737.5	1.599 ± 0.082	7.789 ± 0.039	8.086	–1.439 ± 0.025	–0.809 ± 0.013	2.172 ± 0.019	0.715
289	1064- 52577- 509	J032713.08+003112.3	1.184 ± 0.062	8.171 ± 0.050	8.212	–1.320 ± 0.016	–0.859 ± 0.011	2.124 ± 0.014	0.766
290	1067- 52616- 112	J030502.28-000453.7	1.169 ± 0.059	8.161 ± 0.051	8.041	–1.478 ± 0.016	–0.935 ± 0.011	2.268 ± 0.013	0.783
291	1069- 52590- 399	J024359.02+003322.6	1.304 ± 0.036	8.075 ± 0.028	8.108	–1.606 ± 0.020	–1.053 ± 0.012	2.483 ± 0.018	0.830
292	1073- 52649- 409	J021306.62+005612.4	1.427 ± 0.018	7.972 ± 0.021	8.654	–1.555 ± 0.007	–1.259 ± 0.007	2.501 ± 0.005	0.921
293	1073- 52649- 419	J021332.93+010825.8	1.419 ± 0.042	7.973 ± 0.030	8.045	–1.699 ± 0.023	–1.047 ± 0.013	2.602 ± 0.020	0.868
294	1074- 52937- 186	J020551.72-003229.0	1.021 ± 0.057	8.292 ± 0.054	8.602	–1.022 ± 0.006	–0.700 ± 0.006	1.627 ± 0.004	0.620
295	1074- 52937- 573	J020817.62+004358.4	1.145 ± 0.045	8.214 ± 0.040	8.182	–1.440 ± 0.014	–0.995 ± 0.011	2.252 ± 0.012	0.777
296	1081- 52531- 17	J011640.25-004712.8	1.257 ± 0.075	8.141 ± 0.050	8.264	–1.355 ± 0.018	–0.874 ± 0.014	2.140 ± 0.016	0.696
297	1083- 52520- 354	J005410.34+003812.4	1.259 ± 0.078	8.120 ± 0.059	8.143	–1.546 ± 0.036	–1.109 ± 0.026	2.443 ± 0.033	0.858
298	1084- 52591- 99	J005132.11-004608.0	1.343 ± 0.097	7.957 ± 0.062	7.923	–2.024 ± 0.070	–1.082 ± 0.019	2.792 ± 0.068	0.794
299	1093- 52591- 261	J233817.90-001157.4	1.212 ± 0.071	8.175 ± 0.054	8.268	–1.338 ± 0.013	–0.889 ± 0.009	2.154 ± 0.010	0.739
300	1094- 52524- 543	J233549.15+001314.8	1.426 ± 0.069	7.887 ± 0.043	7.882	–1.746 ± 0.061	–1.284 ± 0.054	2.558 ± 0.059	0.853
301	1095- 52521- 381	J232122.52+003455.2	1.217 ± 0.071	8.154 ± 0.057	8.122	–1.558 ± 0.029	–0.988 ± 0.018	2.408 ± 0.025	0.803
302	1095- 52521- 619	J232757.74+005819.2	1.279 ± 0.096	8.067 ± 0.067	8.075	–1.596 ± 0.034	–0.940 ± 0.017	2.394 ± 0.031	0.770
303	1096- 52974- 102	J231845.21-002610.3	1.124 ± 0.057	8.224 ± 0.046	8.147	–1.297 ± 0.009	–0.784 ± 0.012	2.035 ± 0.007	0.707
304	1096- 52974- 630	J232122.52+003455.2	1.173 ± 0.061	8.204 ± 0.052	8.103	–1.626 ± 0.024	–1.005 ± 0.013	2.483 ± 0.021	0.811
305	1101- 52621- 576	J224041.33+005703.6	1.257 ± 0.073	8.145 ± 0.052	8.334	–1.400 ± 0.027	–0.986 ± 0.021	2.265 ± 0.025	0.785
306	1104- 52912- 439	J221243.06+000648.6	1.141 ± 0.061	8.221 ± 0.053	8.505	–1.278 ± 0.035	–0.965 ± 0.024	2.102 ± 0.033	0.806
307	1104- 52912- 511	J221523.06+000246.6	1.304 ± 0.019	8.093 ± 0.020	8.711	–1.350 ± 0.007	–1.162 ± 0.010	2.280 ± 0.005	0.877
308	1116- 52932- 12	J205034.66-004619.9	1.486 ± 0.095	7.867 ± 0.045	8.000	–1.528 ± 0.032	–0.902 ± 0.021	2.213 ± 0.029	0.671
309	1116- 52932- 89	J204827.46-005958.5	1.615 ± 0.060	7.723 ± 0.030	7.896	–1.828 ± 0.028	–1.089 ± 0.013	2.574 ± 0.026	0.801
310	1156- 52641- 378	J033128.49+003737.5	1.392 ± 0.065	7.919 ± 0.037	7.991	–1.506 ± 0.019	–0.891 ± 0.011	2.220 ± 0.017	0.720
311	1156- 52641- 423	J033047.69+002920.4	1.166 ± 0.048	8.187 ± 0.038	8.176	–1.360 ± 0.012	–0.880 ± 0.009	2.125 ± 0.010	0.724
312	1158- 52668- 370	J135013.80+585313.5	1.175 ± 0.085	8.113 ± 0.064	8.217	–1.160 ± 0.011	–0.716 ± 0.010	1.774 ± 0.008	0.619
313	1160- 52674- 534	J141652.46+571215.8	1.103 ± 0.057	8.223 ± 0.048	8.157	–1.212 ± 0.012	–0.719 ± 0.011	1.902 ± 0.010	0.675
314	1163- 52669- 284	J144328.47+533919.0	1.221 ± 0.031	8.121 ± 0.024	8.577	–1.259 ± 0.008	–0.925 ± 0.007	2.049 ± 0.006	0.764
315	1168- 52731- 639	J155548.46+465715.8	1.243 ± 0.078	8.080 ± 0.055	8.135	–1.238 ± 0.013	–0.697 ± 0.009	1.913 ± 0.010	0.644
316	1170- 52756- 485	J160821.94+432738.5	1.041 ± 0.064	8.309 ± 0.063	8.579	–1.157 ± 0.009	–0.815 ± 0.011	1.882 ± 0.007	0.714

Table 1. continued.

(1)	(2)	(3)	(4)	(5)	(6)	(7)	(8)	(9)	(10)
Num	Plate-MJD-FiberID	IAU designations	t_3 (10^4K)	12+log(O/H)$_{T_e}$	(O/H)$_{\rm Bay}$	N2	S2	O3N2	P
317	1176- 52791- 591	J165712.75+321141.2	1.208 ± 0.031	8.094 ± 0.025	8.097	–1.344 ± 0.008	–0.894 ± 0.007	2.085 ± 0.006	0.751
318	1177- 52824- 556	J214350.86-072003.8	1.388 ± 0.044	7.950 ± 0.028	8.551	–1.299 ± 0.013	–0.957 ± 0.011	2.097 ± 0.011	0.793
319	1177- 52824- 616	J214338.30-065034.8	1.155 ± 0.061	8.179 ± 0.048	8.221	–1.215 ± 0.009	–0.755 ± 0.009	1.912 ± 0.005	0.665
320	1184- 52641- 581	J082057.60+034503.6	1.049 ± 0.064	8.296 ± 0.058	8.584	–1.091 ± 0.007	–0.735 ± 0.006	1.740 ± 0.005	0.624
321	1192- 52649- 173	J090356.79+045613.5	1.238 ± 0.041	8.086 ± 0.031	8.411	–1.310 ± 0.022	–0.948 ± 0.011	2.093 ± 0.019	0.775
322	1195- 52724- 60	J092540.94+063116.6	1.198 ± 0.040	8.163 ± 0.031	8.112	–1.419 ± 0.011	–0.862 ± 0.008	2.204 ± 0.008	0.734
323	1199- 52703- 600	J090610.83+395335.1	1.170 ± 0.050	8.171 ± 0.035	8.278	–1.151 ± 0.009	–0.679 ± 0.006	1.805 ± 0.006	0.608
324	1203- 52669- 570	J074915.48+225342.3	0.983 ± 0.054	8.417 ± 0.056	8.539	–1.163 ± 0.008	–0.777 ± 0.007	1.850 ± 0.005	0.635
325	1205- 52670- 307	J075838.40+252558.4	1.018 ± 0.055	8.265 ± 0.052	8.797	–0.938 ± 0.006	–0.873 ± 0.007	1.526 ± 0.004	0.640
326	1207- 52672- 506	J082527.65+295739.2	1.001 ± 0.048	8.368 ± 0.046	8.346	–1.129 ± 0.007	–0.679 ± 0.006	1.761 ± 0.005	0.597
327	1212- 52703- 388	J090403.60+363914.0	1.137 ± 0.036	8.238 ± 0.030	8.124	–1.411 ± 0.011	–0.854 ± 0.008	2.178 ± 0.008	0.702
328	1212- 52703- 584	J091208.95+362226.4	1.281 ± 0.029	8.061 ± 0.022	8.641	–1.230 ± 0.009	–0.993 ± 0.011	2.033 ± 0.007	0.781
329	1213- 52972- 88	J091724.07+362618.9	0.974 ± 0.050	8.397 ± 0.053	8.552	–1.152 ± 0.008	–0.773 ± 0.007	1.824 ± 0.005	0.653
330	1213- 52972- 500	J091640.05+373159.5	1.277 ± 0.039	8.105 ± 0.028	8.136	–1.464 ± 0.015	–0.903 ± 0.010	2.289 ± 0.013	0.758
331	1214- 52731- 339	J092126.45+384619.2	0.996 ± 0.047	8.344 ± 0.050	8.653	–1.050 ± 0.007	–0.879 ± 0.008	1.753 ± 0.005	0.721
332	1215- 52725- 273	J093538.86+383754.4	1.187 ± 0.024	8.205 ± 0.025	8.786	–1.440 ± 0.011	–1.131 ± 0.013	2.345 ± 0.009	0.859
333	1215- 52725- 629	J094314.40+403842.7	1.078 ± 0.062	8.282 ± 0.051	8.581	–1.035 ± 0.008	–0.682 ± 0.007	1.657 ± 0.005	0.569
334	1217- 52672- 271	J095538.93+414320.6	1.040 ± 0.065	8.328 ± 0.064	8.111	–1.341 ± 0.013	–0.830 ± 0.009	2.083 ± 0.010	0.709
335	1223- 52781- 287	J112437.80+083112.7	1.237 ± 0.069	8.074 ± 0.047	8.573	–1.098 ± 0.009	–0.739 ± 0.007	1.773 ± 0.006	0.661
336	1224- 52765- 566	J114025.94+104653.7	1.191 ± 0.074	8.167 ± 0.056	8.290	–1.252 ± 0.014	–0.804 ± 0.013	2.012 ± 0.011	0.708
337	1233- 52734- 335	J123444.26+104308.7	1.219 ± 0.033	8.158 ± 0.026	8.119	–1.494 ± 0.011	–0.905 ± 0.007	2.296 ± 0.007	0.736
338	1237- 52762- 42	J101629.88+073404.8	1.173 ± 0.035	8.211 ± 0.029	8.722	–1.088 ± 0.008	–0.922 ± 0.012	1.920 ± 0.007	0.774
339	1240- 52734- 340	J103509.33+094516.9	1.070 ± 0.039	8.263 ± 0.039	8.596	–1.207 ± 0.009	–0.914 ± 0.009	1.962 ± 0.006	0.761
340	1268- 52933- 318	J083038.23+285852.6	1.089 ± 0.044	8.226 ± 0.041	8.884	–0.890 ± 0.006	–0.953 ± 0.009	1.624 ± 0.004	0.755
341	1269- 52937- 177	J084219.08+300703.7	1.046 ± 0.039	8.280 ± 0.038	8.623	–1.113 ± 0.006	–0.877 ± 0.008	1.816 ± 0.004	0.711
342	1274- 52995- 258	J092125.53+345858.4	1.134 ± 0.060	8.212 ± 0.048	8.417	–1.161 ± 0.010	–0.737 ± 0.011	1.870 ± 0.008	0.669
343	1279- 52736- 147	J125153.04+493216.7	1.158 ± 0.056	8.193 ± 0.048	8.128	–1.377 ± 0.012	–0.871 ± 0.009	2.148 ± 0.007	0.733
344	1283- 52762- 315	J132751.58+480805.2	1.080 ± 0.048	8.250 ± 0.045	8.572	–1.122 ± 0.009	–0.829 ± 0.008	1.850 ± 0.006	0.724
345	1286- 52725- 150	J141020.62+460501.6	1.210 ± 0.045	8.133 ± 0.032	8.507	–1.091 ± 0.008	–0.740 ± 0.007	1.816 ± 0.006	0.681
346	1286- 52725- 579	J141121.91+472849.4	1.124 ± 0.052	8.232 ± 0.042	8.331	–1.190 ± 0.010	–0.741 ± 0.008	1.905 ± 0.007	0.666
347	1301- 52976- 356	J090934.68+085837.5	1.041 ± 0.054	8.272 ± 0.043	8.671	–0.888 ± 0.004	–0.681 ± 0.005	1.416 ± 0.003	0.535
348	1303- 53050- 66	J093623.28+090001.0	1.166 ± 0.056	8.201 ± 0.049	8.701	–1.211 ± 0.015	–0.979 ± 0.017	2.066 ± 0.013	0.822
349	1304- 52993- 245	J093317.21+085425.9	1.153 ± 0.074	8.153 ± 0.052	8.607	–0.909 ± 0.007	–0.665 ± 0.006	1.484 ± 0.004	0.561
350	1306- 52996- 292	J094756.86+091132.2	1.403 ± 0.032	7.930 ± 0.023	7.987	–1.735 ± 0.018	–1.087 ± 0.010	2.549 ± 0.015	0.826
351	1310- 53033- 508	J113734.87+572406.1	1.107 ± 0.047	8.252 ± 0.040	8.132	–1.319 ± 0.013	–0.787 ± 0.008	2.065 ± 0.010	0.704
352	1316- 52790- 581	J123801.22+580114.5	1.367 ± 0.024	8.057 ± 0.022	8.367	–1.575 ± 0.012	–1.146 ± 0.014	2.530 ± 0.009	0.885
353	1324- 53088- 524	J140721.21+553807.8	1.001 ± 0.057	8.387 ± 0.058	8.590	–1.141 ± 0.009	–0.817 ± 0.016	1.861 ± 0.007	0.683
354	1325- 52762- 519	J141431.20+543056.1	1.260 ± 0.059	8.091 ± 0.043	8.256	–1.406 ± 0.027	–1.020 ± 0.026	2.234 ± 0.025	0.799
355	1326- 52764- 377	J142344.91+535924.7	1.308 ± 0.067	8.029 ± 0.045	8.092	–1.416 ± 0.019	–0.835 ± 0.012	2.192 ± 0.016	0.755
356	1331- 52766- 258	J152115.67+465840.8	1.290 ± 0.090	7.948 ± 0.054	8.696	–0.903 ± 0.010	–0.727 ± 0.011	1.447 ± 0.008	0.598
357	1331- 52766- 554	J152841.69+475445.7	1.247 ± 0.032	8.075 ± 0.028	8.362	–1.445 ± 0.012	–1.063 ± 0.011	2.262 ± 0.009	0.822
358	1332- 52781- 27	J154120.02+453619.0	1.016 ± 0.051	8.345 ± 0.053	8.846	–0.956 ± 0.009	–0.915 ± 0.011	1.713 ± 0.007	0.756
359	1332- 52781- 602	J153821.29+465103.6	1.492 ± 0.137	7.870 ± 0.066	8.242	–1.197 ± 0.019	–0.734 ± 0.018	1.867 ± 0.016	0.633
360	1333- 52782- 172	J154544.52+441551.8	1.281 ± 0.048	8.075 ± 0.033	8.107	–1.462 ± 0.014	–0.901 ± 0.010	2.239 ± 0.011	0.727
361	1335- 52824- 291	J155944.57+403325.2	1.195 ± 0.053	8.167 ± 0.045	8.310	–1.369 ± 0.021	–0.995 ± 0.020	2.221 ± 0.019	0.820
362	1338- 52765- 329	J162350.72+371003.7	1.106 ± 0.036	8.290 ± 0.034	8.509	–1.329 ± 0.010	–0.965 ± 0.011	2.152 ± 0.008	0.756
363	1345- 52814- 364	J134251.19+441343.3	1.068 ± 0.065	8.268 ± 0.064	8.171	–1.335 ± 0.014	–0.882 ± 0.011	2.100 ± 0.011	0.770
364	1349- 52797- 175	J143248.38+395917.8	1.224 ± 0.021	8.148 ± 0.019	8.434	–1.393 ± 0.009	–0.993 ± 0.008	2.245 ± 0.007	0.807
365	1349- 52797- 429	J143036.00+402413.6	1.193 ± 0.065	8.186 ± 0.051	8.187	–1.396 ± 0.018	–0.907 ± 0.013	2.206 ± 0.015	0.743
366	1355- 52823- 98	J153536.14+332843.3	0.984 ± 0.052	8.441 ± 0.059	8.531	–1.209 ± 0.008	–0.850 ± 0.008	1.978 ± 0.004	0.700
367	1356- 53033- 248	J100052.15+383056.8	1.016 ± 0.051	8.347 ± 0.052	8.573	–0.988 ± 0.007	–0.783 ± 0.009	1.699 ± 0.005	0.690
368	1357- 53034- 245	J101207.44+393132.1	1.080 ± 0.071	8.286 ± 0.062	8.489	–1.085 ± 0.035	–0.767 ± 0.010	1.820 ± 0.034	0.692
369	1357- 53034- 540	J101541.16+412050.2	1.037 ± 0.042	8.357 ± 0.044	8.585	–1.209 ± 0.009	–0.960 ± 0.009	2.015 ± 0.006	0.760

Table 1. continued.

(1)	(2)	(3)	(4)	(5)	(6)	(7)	(8)	(9)	(10)
Num	Plate-MJD-FiberID	IAU designations	t_3 (10^4K)	12+log(O/H)$_{T_e}$	(O/H)$_{\rm Bay}$	N2	S2	O3N2	P
370	1357- 53034- 579	J101803.24+410621.2	1.407 ± 0.036	7.979 ± 0.026	8.649	–1.440 ± 0.023	–1.186 ± 0.032	2.340 ± 0.021	0.872
371	1363- 53053- 411	J110251.98+433827.2	1.135 ± 0.045	8.206 ± 0.036	8.077	–1.390 ± 0.012	–0.817 ± 0.008	2.117 ± 0.009	0.696
372	1363- 53053- 599	J110744.09+443825.8	1.074 ± 0.058	8.286 ± 0.053	8.423	–1.221 ± 0.010	–0.805 ± 0.009	1.948 ± 0.006	0.688
373	1365- 53062- 381	J111727.26+450043.2	1.349 ± 0.031	8.072 ± 0.029	8.182	–1.518 ± 0.024	–1.322 ± 0.030	2.497 ± 0.022	0.919
374	1368- 53084- 334	J114424.02+443630.2	1.102 ± 0.055	8.198 ± 0.046	8.505	–1.167 ± 0.010	–0.773 ± 0.007	1.827 ± 0.007	0.673
375	1372- 53062- 517	J123915.79+444800.7	0.964 ± 0.045	8.368 ± 0.049	8.622	–0.969 ± 0.006	–0.776 ± 0.006	1.607 ± 0.004	0.666
376	1382- 53115- 231	J143532.88+364630.7	1.295 ± 0.087	8.010 ± 0.053	8.243	–1.183 ± 0.015	–0.755 ± 0.010	1.825 ± 0.013	0.629
377	1388- 53119- 39	J153656.45+312248.0	1.088 ± 0.052	8.260 ± 0.045	8.589	–1.110 ± 0.007	–0.829 ± 0.007	1.811 ± 0.004	0.666
378	1391- 52817- 231	J155338.85+280257.8	1.074 ± 0.068	8.222 ± 0.054	8.780	–0.708 ± 0.005	–0.696 ± 0.006	1.241 ± 0.003	0.547
379	1394- 53108- 259	J141240.42+424213.3	1.210 ± 0.090	8.156 ± 0.062	8.146	–1.290 ± 0.013	–0.695 ± 0.010	1.978 ± 0.011	0.613
380	1395- 52825- 242	J142405.74+421646.2	1.353 ± 0.018	8.059 ± 0.019	8.786	–1.330 ± 0.009	–1.180 ± 0.012	2.276 ± 0.007	0.889
381	1398- 53146- 573	J150321.55+401652.6	1.494 ± 0.138	7.863 ± 0.069	8.134	–1.280 ± 0.021	–0.731 ± 0.017	1.948 ± 0.017	0.636
382	1399- 53172- 204	J151242.96+372535.0	1.067 ± 0.068	8.321 ± 0.068	8.550	–1.248 ± 0.018	–0.956 ± 0.017	2.070 ± 0.015	0.776
383	1401- 53144- 397	J152821.98+362409.3	1.069 ± 0.042	8.323 ± 0.043	8.543	–1.290 ± 0.011	–0.968 ± 0.010	2.126 ± 0.008	0.791
384	1405- 52826- 395	J160135.95+311353.7	1.021 ± 0.061	8.335 ± 0.063	8.585	–1.135 ± 0.010	–0.842 ± 0.010	1.861 ± 0.007	0.715
385	1409- 52824- 461	J163305.62+260026.6	1.920 ± 0.219	7.595 ± 0.068	8.046	–1.539 ± 0.045	–0.805 ± 0.021	2.183 ± 0.041	0.617
386	1418- 53142- 442	J160055.10+344551.8	1.155 ± 0.055	8.138 ± 0.042	8.615	–1.051 ± 0.008	–0.794 ± 0.008	1.712 ± 0.006	0.672
387	1425- 52913- 518	J170450.35+204718.9	1.052 ± 0.053	8.359 ± 0.053	8.500	–1.247 ± 0.011	–0.886 ± 0.010	2.056 ± 0.009	0.738
388	1428- 52998- 568	J102847.64+394941.5	0.923 ± 0.047	8.515 ± 0.055	8.623	–1.071 ± 0.007	–0.759 ± 0.006	1.695 ± 0.004	0.558
389	1430- 53002- 389	J102909.31+394426.1	0.955 ± 0.046	8.401 ± 0.052	8.602	–1.108 ± 0.007	–0.815 ± 0.007	1.780 ± 0.005	0.684
390	1442- 53050- 396	J112546.80+470000.3	0.865 ± 0.044	8.557 ± 0.059	8.688	–0.963 ± 0.005	–0.846 ± 0.006	1.627 ± 0.003	0.665
391	1445- 53062- 429	J114138.04+423437.2	1.299 ± 0.060	8.024 ± 0.039	8.065	–1.365 ± 0.015	–0.837 ± 0.011	2.093 ± 0.013	0.709
392	1454- 53090- 204	J123506.50+413736.4	0.975 ± 0.058	8.358 ± 0.062	8.735	–0.902 ± 0.007	–0.800 ± 0.009	1.556 ± 0.005	0.679
393	1455- 53089- 287	J123803.77+461820.1	1.243 ± 0.026	8.153 ± 0.022	8.662	–1.262 ± 0.008	–0.979 ± 0.008	2.135 ± 0.005	0.800
394	1457- 53116- 381	J125251.63+480508.1	1.059 ± 0.068	8.340 ± 0.064	8.225	–1.307 ± 0.016	–0.825 ± 0.010	2.063 ± 0.013	0.680
395	1462- 53112- 184	J132032.04+405901.6	1.020 ± 0.064	8.326 ± 0.063	8.708	–1.041 ± 0.008	–0.897 ± 0.009	1.717 ± 0.006	0.671
396	1464- 53091- 232	J133037.68+401953.0	1.016 ± 0.041	8.356 ± 0.042	8.156	–1.304 ± 0.008	–0.821 ± 0.008	2.037 ± 0.006	0.706
397	1464- 53091- 442	J133346.30+415213.0	1.138 ± 0.064	8.226 ± 0.050	8.460	–1.131 ± 0.011	–0.727 ± 0.008	1.828 ± 0.008	0.633
398	1466- 53083- 92	J135403.26+442616.4	1.065 ± 0.063	8.296 ± 0.057	8.588	–1.090 ± 0.008	–0.797 ± 0.008	1.780 ± 0.005	0.645
399	1467- 53115- 32	J141022.27+441455.6	1.079 ± 0.066	8.244 ± 0.059	8.296	–1.183 ± 0.009	–0.752 ± 0.008	1.851 ± 0.007	0.660
400	1467- 53115- 579	J141007.10+450817.5	1.057 ± 0.047	8.274 ± 0.038	8.597	–0.975 ± 0.006	–0.674 ± 0.006	1.563 ± 0.003	0.570
401	1474- 52933- 51	J220200.67-011208.6	1.302 ± 0.060	8.041 ± 0.043	8.056	–1.621 ± 0.029	–0.955 ± 0.016	2.436 ± 0.027	0.795
402	1476- 52964- 530	J221549.25+010938.8	1.077 ± 0.052	8.264 ± 0.049	8.091	–1.347 ± 0.013	–0.803 ± 0.009	2.098 ± 0.011	0.742
403	1487- 52964- 510	J234249.56+002440.3	1.309 ± 0.049	8.011 ± 0.034	8.025	–1.519 ± 0.032	–0.939 ± 0.011	2.300 ± 0.030	0.783
404	1491- 52996- 350	J000938.35+002535.7	1.546 ± 0.147	7.801 ± 0.070	8.093	–1.416 ± 0.044	–0.835 ± 0.020	2.156 ± 0.041	0.755
405	1492- 52932- 10	J002425.03-010359.0	1.498 ± 0.046	7.895 ± 0.032	7.998	–1.808 ± 0.028	–1.180 ± 0.016	2.705 ± 0.025	0.884
406	1495- 52944- 627	J004829.64+003710.5	1.369 ± 0.049	7.983 ± 0.031	8.082	–1.514 ± 0.019	–0.892 ± 0.009	2.276 ± 0.014	0.724
407	1522- 52932- 40	J212657.96-003227.9	1.713 ± 0.152	7.744 ± 0.062	8.124	–1.562 ± 0.049	–0.902 ± 0.031	2.359 ± 0.047	0.760
408	1562- 53052- 557	J025754.79+002726.6	1.250 ± 0.043	8.179 ± 0.036	8.116	–1.581 ± 0.023	–1.066 ± 0.017	2.528 ± 0.021	0.855
409	1570- 53149- 146	J164202.38+210345.7	1.067 ± 0.045	8.219 ± 0.039	8.816	–0.801 ± 0.005	–0.798 ± 0.005	1.420 ± 0.002	0.654
410	1571- 53174- 155	J163527.94+222518.8	0.959 ± 0.053	8.413 ± 0.060	8.557	–1.200 ± 0.007	–0.821 ± 0.007	1.893 ± 0.005	0.690
411	1580- 53145- 418	J154613.87+330423.1	1.087 ± 0.048	8.241 ± 0.044	8.592	–1.090 ± 0.008	–0.841 ± 0.008	1.814 ± 0.005	0.718
412	1580- 53145- 419	J154659.02+325632.2	1.277 ± 0.034	8.110 ± 0.030	8.137	–1.543 ± 0.030	–1.196 ± 0.016	2.463 ± 0.028	0.879
413	1584- 52943- 372	J080824.94+230840.9	0.981 ± 0.048	8.413 ± 0.048	8.780	–0.846 ± 0.006	–0.826 ± 0.007	1.542 ± 0.004	0.654
414	1584- 52943- 486	J080911.47+224758.9	1.113 ± 0.069	8.238 ± 0.050	8.575	–0.973 ± 0.007	–0.635 ± 0.010	1.555 ± 0.005	0.527
415	1590- 52974- 628	J090405.90+313045.0	1.332 ± 0.082	7.921 ± 0.047	8.613	–1.022 ± 0.008	–0.725 ± 0.009	1.614 ± 0.005	0.635
416	1595- 52999- 532	J095115.96+364031.0	1.041 ± 0.061	8.267 ± 0.053	8.623	–0.914 ± 0.006	–0.676 ± 0.006	1.469 ± 0.004	0.561
417	1597- 52999- 50	J101828.39+095412.2	1.021 ± 0.063	8.270 ± 0.060	8.663	–0.994 ± 0.006	–0.768 ± 0.006	1.588 ± 0.004	0.636
418	1597- 52999- 168	J101546.87+101234.5	1.131 ± 0.076	8.230 ± 0.064	8.189	–1.304 ± 0.020	–0.806 ± 0.012	2.062 ± 0.017	0.711
419	1597- 52999- 251	J101139.17+101042.2	1.059 ± 0.053	8.325 ± 0.051	8.120	–1.366 ± 0.013	–0.811 ± 0.009	2.123 ± 0.010	0.703
420	1597- 52999- 358	J100950.23+110439.3	1.024 ± 0.042	8.301 ± 0.042	8.598	–1.153 ± 0.007	–0.830 ± 0.007	1.851 ± 0.005	0.717
421	1601- 53115- 168	J104829.23+111520.1	1.224 ± 0.027	8.161 ± 0.024	8.161	–1.421 ± 0.010	–0.909 ± 0.012	2.295 ± 0.008	0.815
422	1601- 53115- 526	J104819.42+123745.8	1.324 ± 0.103	7.944 ± 0.059	8.627	–1.048 ± 0.015	–0.717 ± 0.017	1.623 ± 0.012	0.598
423	1607- 53083- 205	J113530.91+111717.8	1.104 ± 0.040	8.245 ± 0.036	8.112	–1.327 ± 0.011	–0.819 ± 0.008	2.077 ± 0.009	0.721

Table 1. continued.

(1)	(2)	(3)	(4)	(5)	(6)	(7)	(8)	(9)	(10)
Num	Plate-MJD-FiberID	IAU designations	t_3 (10^4K)	12+log(O/H)$_{T_e}$	(O/H)$_{Bay}$	N2	S2	O3N2	P
424	1609- 53142- 238	J114837.49+121407.8	1.170 ± 0.045	8.142 ± 0.036	8.041	–1.360 ± 0.010	–0.861 ± 0.008	2.096 ± 0.008	0.738
425	1615- 53166- 206	J122900.39+112302.0	1.105 ± 0.069	8.247 ± 0.061	8.536	–1.148 ± 0.011	–0.789 ± 0.010	1.879 ± 0.008	0.693
426	1616- 53169- 205	J123534.25+111926.0	1.151 ± 0.039	8.247 ± 0.034	8.118	–1.410 ± 0.014	–0.875 ± 0.009	2.237 ± 0.011	0.745
427	1620- 53137- 470	J114228.75+075709.3	0.991 ± 0.059	8.403 ± 0.062	8.498	–1.232 ± 0.012	–0.844 ± 0.015	1.974 ± 0.009	0.706
428	1623- 53089- 493	J120344.83+072903.8	1.234 ± 0.089	8.071 ± 0.062	8.099	–1.268 ± 0.015	–0.694 ± 0.011	1.918 ± 0.012	0.638
429	1632- 52996- 135	J034254.29-005520.2	1.124 ± 0.045	8.229 ± 0.039	8.190	–1.341 ± 0.022	–0.910 ± 0.011	2.132 ± 0.021	0.762
430	1644- 53144- 564	J142805.52+362710.4	1.418 ± 0.022	7.941 ± 0.017	8.065	–1.502 ± 0.009	–1.029 ± 0.008	2.333 ± 0.006	0.816
431	1648- 53171- 21	J150950.07+314639.7	1.238 ± 0.076	8.084 ± 0.057	8.042	–1.439 ± 0.018	–0.868 ± 0.013	2.191 ± 0.015	0.739
432	1650- 53174- 305	J151634.77+300653.6	0.988 ± 0.044	8.387 ± 0.047	8.498	–1.098 ± 0.007	–0.832 ± 0.006	1.812 ± 0.004	0.694
433	1682- 53173- 3	J160810.37+352809.1	1.800 ± 0.039	7.745 ± 0.031	7.879	–2.528 ± 0.054	–1.833 ± 0.032	3.529 ± 0.047	0.980
434	1689- 53177- 521	J171108.98+234547.1	1.279 ± 0.049	8.075 ± 0.034	8.094	–1.515 ± 0.017	–0.897 ± 0.010	2.312 ± 0.015	0.756
435	1697- 53142- 48	J131644.79+105733.1	1.123 ± 0.033	8.259 ± 0.033	8.188	–1.425 ± 0.018	–0.959 ± 0.009	2.275 ± 0.016	0.805
436	1702- 53144- 62	J135832.26+104718.9	1.202 ± 0.025	8.222 ± 0.026	8.794	–1.466 ± 0.011	–1.199 ± 0.011	2.414 ± 0.008	0.867
437	1704- 53178- 345	J140158.15+134830.2	1.177 ± 0.069	8.163 ± 0.049	8.277	–1.180 ± 0.010	–0.716 ± 0.010	1.841 ± 0.007	0.613
438	1704- 53178- 478	J140555.23+140528.3	1.185 ± 0.077	8.149 ± 0.055	8.159	–1.248 ± 0.014	–0.741 ± 0.010	1.922 ± 0.012	0.634
439	1734- 53034- 490	J073149.49+404513.3	1.224 ± 0.031	8.145 ± 0.028	8.106	–1.549 ± 0.012	–1.013 ± 0.008	2.409 ± 0.009	0.820
440	1744- 53055- 450	J100307.77+130326.2	1.015 ± 0.061	8.339 ± 0.058	8.614	–0.991 ± 0.007	–0.742 ± 0.007	1.630 ± 0.004	0.618
441	1745- 53061- 463	J101157.09+130822.2	1.437 ± 0.018	8.000 ± 0.019	8.361	–1.644 ± 0.013	–1.349 ± 0.013	2.622 ± 0.011	0.918
442	1747- 53075- 182	J102744.14+130934.2	1.043 ± 0.054	8.307 ± 0.053	8.589	–1.039 ± 0.007	–0.817 ± 0.008	1.772 ± 0.005	0.720
443	1758- 53084- 338	J082520.11+082723.0	1.122 ± 0.042	8.265 ± 0.040	8.379	–1.423 ± 0.014	–1.016 ± 0.016	2.287 ± 0.011	0.818
444	1821- 53167- 496	J154453.28+062452.9	1.314 ± 0.089	7.985 ± 0.056	8.034	–1.337 ± 0.017	–0.770 ± 0.013	2.016 ± 0.015	0.681
445	282- 51630- 546	J113703.79+002817.4	1.156 ± 0.034	8.248 ± 0.031	8.186	–1.443 ± 0.018	–0.916 ± 0.010	2.333 ± 0.016	0.822
446	296- 51665- 411	J131937.25+005043.8	1.062 ± 0.037	8.346 ± 0.038	8.485	–1.364 ± 0.012	–0.995 ± 0.010	2.199 ± 0.008	0.770
447	297- 51663- 446	J132654.62+011346.5	1.209 ± 0.028	8.135 ± 0.025	8.103	–1.445 ± 0.012	–0.977 ± 0.012	2.286 ± 0.011	0.828
448	301- 51641- 525	J140018.94+010453.7	1.232 ± 0.025	8.124 ± 0.021	8.536	–1.303 ± 0.008	–0.955 ± 0.008	2.135 ± 0.006	0.799
449	304- 51609- 583	J142200.19+010213.2	1.011 ± 0.053	8.359 ± 0.052	8.553	–1.189 ± 0.008	–0.800 ± 0.011	1.893 ± 0.006	0.677
450	309- 51666- 282	J145146.99-005643.8	1.162 ± 0.026	8.188 ± 0.023	8.067	–1.545 ± 0.013	–0.976 ± 0.008	2.346 ± 0.011	0.773
451	348- 51696- 339	J163107.20+005324.7	1.168 ± 0.061	8.177 ± 0.047	8.088	–1.384 ± 0.011	–0.828 ± 0.008	2.116 ± 0.009	0.692
452	351- 51695- 217	J170201.44+604746.3	1.034 ± 0.041	8.293 ± 0.035	8.624	–0.961 ± 0.005	–0.747 ± 0.005	1.568 ± 0.003	0.602
453	394- 51812- 480	J005147.30+000939.9	1.566 ± 0.023	7.782 ± 0.018	7.866	–1.880 ± 0.024	–1.260 ± 0.010	2.709 ± 0.022	0.880
454	394- 51876- 472	J005147.30+000939.9	1.548 ± 0.018	7.797 ± 0.017	7.864	–1.873 ± 0.018	–1.289 ± 0.009	2.718 ± 0.016	0.898
455	406- 51817- 490	J022407.68+003226.1	1.085 ± 0.070	8.263 ± 0.059	8.125	–1.272 ± 0.011	–0.708 ± 0.007	1.919 ± 0.008	0.607
456	406- 51900- 204	J022312.62-004539.9	1.432 ± 0.125	7.906 ± 0.063	8.499	–1.015 ± 0.013	–0.630 ± 0.012	1.597 ± 0.010	0.550
457	406- 51900- 488	J022407.68+003226.1	1.183 ± 0.068	8.158 ± 0.048	8.130	–1.281 ± 0.011	–0.709 ± 0.008	1.920 ± 0.008	0.588
458	414- 51869- 459	J032724.17+004804.3	1.026 ± 0.051	8.310 ± 0.047	8.661	–1.086 ± 0.007	–0.841 ± 0.009	1.751 ± 0.005	0.667
459	414- 51869- 524	J032750.16+010135.0	1.040 ± 0.061	8.343 ± 0.054	8.445	–1.131 ± 0.008	–0.720 ± 0.007	1.788 ± 0.006	0.593
460	415- 51879- 284	J033031.22-005846.5	1.139 ± 0.039	8.250 ± 0.037	8.132	–1.518 ± 0.016	–0.991 ± 0.009	2.382 ± 0.014	0.807
461	419- 51812- 362	J004236.94+160202.7	1.059 ± 0.064	8.319 ± 0.063	8.821	–1.105 ± 0.012	–1.050 ± 0.028	1.931 ± 0.010	0.800
462	419- 51868- 362	J004236.94+160202.7	1.004 ± 0.059	8.393 ± 0.066	8.826	–1.063 ± 0.011	–1.107 ± 0.040	1.894 ± 0.010	0.809
463	425- 51884- 635	J013700.31+144157.1	1.028 ± 0.063	8.301 ± 0.063	8.052	–1.295 ± 0.009	–0.779 ± 0.006	2.001 ± 0.007	0.719
464	437- 51876- 460	J080147.11+435302.0	1.094 ± 0.034	8.271 ± 0.031	8.584	–1.236 ± 0.008	–0.912 ± 0.009	2.017 ± 0.006	0.746
465	483- 51942- 474	J090047.45+574255.0	0.985 ± 0.048	8.409 ± 0.053	8.767	–1.053 ± 0.006	–0.934 ± 0.009	1.830 ± 0.004	0.754
466	483- 51942- 586	J090139.89+575945.9	1.114 ± 0.045	8.235 ± 0.037	8.127	–1.317 ± 0.008	–0.813 ± 0.007	2.048 ± 0.006	0.697
467	594- 52027- 516	J154654.55+030902.1	1.109 ± 0.034	8.286 ± 0.032	8.532	–1.302 ± 0.012	–0.968 ± 0.011	2.149 ± 0.010	0.788
468	616- 52442- 336	J153534.13+545534.3	1.083 ± 0.054	8.314 ± 0.047	8.568	–1.125 ± 0.009	–0.832 ± 0.019	1.913 ± 0.007	0.726
469	662- 52178- 466	J013258.54-085337.6	1.003 ± 0.041	8.381 ± 0.042	8.349	–1.147 ± 0.007	–0.700 ± 0.007	1.844 ± 0.002	0.656
470	673- 52162- 73	J223126.30-000456.2	1.038 ± 0.065	8.328 ± 0.062	8.575	–1.100 ± 0.008	–0.776 ± 0.007	1.797 ± 0.005	0.657
471	675- 52590- 39	J225059.28+000032.7	1.763 ± 0.049	7.697 ± 0.032	7.909	–1.639 ± 0.014	–1.445 ± 0.034	2.543 ± 0.007	0.934
472	676- 52178- 192	J225059.28+000032.7	1.628 ± 0.033	7.758 ± 0.023	7.855	–1.687 ± 0.013	–1.398 ± 0.023	2.559 ± 0.011	0.916
473	677- 52606- 374	J225833.74+005630.4	1.247 ± 0.095	8.088 ± 0.070	8.319	–1.290 ± 0.023	–0.912 ± 0.023	2.093 ± 0.020	0.788
474	677- 52606- 533	J230210.00+004939.0	1.731 ± 0.029	7.655 ± 0.022	7.835	–2.212 ± 0.030	–1.456 ± 0.015	3.039 ± 0.027	0.910
475	678- 52884- 446	J230703.74+011311.2	1.002 ± 0.049	8.334 ± 0.047	8.819	–0.833 ± 0.005	–0.819 ± 0.006	1.467 ± 0.003	0.645
476	681- 52199- 201	J232936.56-011057.0	1.202 ± 0.027	8.176 ± 0.025	8.225	–1.394 ± 0.010	–0.937 ± 0.007	2.255 ± 0.008	0.813
477	681- 52199- 595	J233435.40+002714.4	1.315 ± 0.102	8.038 ± 0.061	8.189	–1.269 ± 0.039	–0.700 ± 0.014	1.927 ± 0.035	0.597

Table 1. continued.

(1)	(2)	(3)	(4)	(5)	(6)	(7)	(8)	(9)	(10)
Num	Plate-MJD-FiberID	IAU designations	t_3 (10^4K)	12+log(O/H)$_{T_e}$	(O/H)$_{\rm Bay}$	N2	S2	O3N2	P
478	682- 52525- 63	J234209.77-002451.1	1.282 ± 0.065	8.103 ± 0.047	8.122	–1.593 ± 0.027	–0.997 ± 0.035	2.448 ± 0.025	0.790
479	682- 52525- 172	J233751.94-001000.4	1.809 ± 0.033	7.738 ± 0.020	8.048	–1.804 ± 0.017	–1.331 ± 0.012	2.748 ± 0.014	0.899
480	683- 52524- 279	J234209.77-002451.1	1.140 ± 0.062	8.251 ± 0.056	8.139	–1.575 ± 0.028	–0.998 ± 0.043	2.443 ± 0.025	0.814
481	684- 52523- 494	J235242.19+002345.9	1.180 ± 0.081	8.146 ± 0.068	8.037	–1.512 ± 0.032	–0.976 ± 0.019	2.315 ± 0.029	0.806
482	684- 52523- 560	J235519.63+000051.8	1.183 ± 0.046	8.187 ± 0.038	8.145	–1.424 ± 0.015	–0.945 ± 0.011	2.226 ± 0.013	0.747
483	685- 52203- 296	J235519.63+000051.8	0.993 ± 0.057	8.387 ± 0.066	8.087	–1.433 ± 0.019	–0.943 ± 0.012	2.236 ± 0.017	0.800
484	686- 52519- 2	J001042.84-010200.9	1.244 ± 0.085	8.161 ± 0.066	8.469	–1.416 ± 0.028	–1.090 ± 0.024	2.339 ± 0.026	0.855
485	686- 52519- 185	J000703.98-003447.6	1.258 ± 0.032	8.117 ± 0.026	8.191	–1.427 ± 0.013	–0.961 ± 0.010	2.272 ± 0.011	0.791
486	686- 52519- 406	J000657.02+005125.9	1.195 ± 0.027	8.177 ± 0.025	8.530	–1.336 ± 0.008	–0.979 ± 0.008	2.181 ± 0.005	0.797
487	686- 52519- 476	J000635.54+002333.3	1.317 ± 0.087	8.037 ± 0.057	8.097	–1.537 ± 0.027	–0.881 ± 0.014	2.341 ± 0.024	0.768
488	691- 52199- 252	J004406.79-010838.4	1.280 ± 0.039	8.110 ± 0.029	8.147	–1.485 ± 0.016	–1.012 ± 0.011	2.353 ± 0.014	0.803
489	691- 52199- 307	J004020.02+000008.6	1.060 ± 0.056	8.221 ± 0.053	8.763	–0.942 ± 0.007	–0.816 ± 0.015	1.629 ± 0.006	0.750
490	691- 52199- 573	J004859.14+005553.0	1.420 ± 0.063	7.928 ± 0.035	8.039	–1.541 ± 0.029	–0.913 ± 0.015	2.312 ± 0.026	0.753
491	691- 52199- 636	J005147.30+000939.9	1.506 ± 0.025	7.833 ± 0.020	7.881	–1.858 ± 0.021	–1.256 ± 0.011	2.695 ± 0.019	0.878
492	692- 52201- 394	J005147.30+000939.9	1.617 ± 0.027	7.768 ± 0.020	7.888	–1.836 ± 0.024	–1.276 ± 0.012	2.683 ± 0.022	0.876
493	693- 52254- 403	J010101.27+011040.0	1.144 ± 0.066	8.225 ± 0.059	8.225	–1.327 ± 0.053	–0.929 ± 0.016	2.171 ± 0.050	0.807
494	693- 52254- 454	J010112.24+005449.3	1.178 ± 0.075	8.173 ± 0.058	8.094	–1.460 ± 0.020	–0.822 ± 0.016	2.206 ± 0.017	0.701
495	693- 52254- 463	J010000.24+001727.2	1.152 ± 0.043	8.259 ± 0.042	8.466	–1.480 ± 0.020	–1.150 ± 0.027	2.410 ± 0.017	0.867
496	693- 52254- 480	J005959.88+000014.0	1.483 ± 0.092	7.857 ± 0.046	8.041	–1.403 ± 0.020	–0.797 ± 0.015	2.108 ± 0.017	0.698
497	694- 52209- 73	J011210.87-000330.9	1.203 ± 0.059	8.154 ± 0.042	8.112	–1.391 ± 0.014	–0.837 ± 0.011	2.161 ± 0.012	0.720
498	694- 52209- 231	J010628.39-002000.9	1.368 ± 0.048	8.036 ± 0.031	8.144	–1.643 ± 0.035	–1.057 ± 0.020	2.531 ± 0.034	0.821
499	695- 52202- 261	J011210.87-000330.9	1.200 ± 0.057	8.168 ± 0.043	8.139	–1.391 ± 0.018	–0.841 ± 0.014	2.164 ± 0.016	0.709
500	698- 52203- 250	J013525.58-011348.3	1.092 ± 0.051	8.262 ± 0.047	8.552	–1.209 ± 0.029	–0.893 ± 0.013	1.982 ± 0.027	0.751
501	699- 52202- 337	J014246.61+010450.5	1.368 ± 0.052	7.963 ± 0.032	8.119	–1.353 ± 0.014	–0.847 ± 0.012	2.117 ± 0.011	0.757
502	701- 52179- 117	J020223.52-002728.0	1.519 ± 0.038	7.820 ± 0.026	7.887	–1.812 ± 0.025	–1.133 ± 0.015	2.638 ± 0.022	0.870
503	702- 52178- 335	J020411.35+004304.8	1.173 ± 0.050	8.171 ± 0.044	8.429	–1.372 ± 0.021	–0.954 ± 0.014	2.194 ± 0.018	0.804
504	703- 52209- 215	J021514.66-005254.4	1.091 ± 0.065	8.298 ± 0.060	8.160	–1.408 ± 0.018	–0.885 ± 0.015	2.227 ± 0.016	0.762
505	704- 52205- 42	J022635.74-011021.3	1.173 ± 0.068	8.186 ± 0.053	8.114	–1.392 ± 0.016	–0.801 ± 0.012	2.163 ± 0.014	0.722
506	704- 52205- 494	J022322.78+002336.9	1.310 ± 0.036	8.037 ± 0.026	8.047	–1.525 ± 0.016	–0.938 ± 0.009	2.351 ± 0.014	0.804
507	707- 52177- 11	J024939.72-011151.3	1.326 ± 0.039	8.035 ± 0.031	8.048	–1.626 ± 0.014	–1.087 ± 0.010	2.492 ± 0.012	0.842
508	707- 52177- 369	J024355.18+011148.8	1.093 ± 0.070	8.287 ± 0.066	8.562	–1.226 ± 0.016	–0.984 ± 0.022	2.059 ± 0.013	0.791
509	707- 52177- 525	J024702.71+011529.5	1.285 ± 0.022	8.099 ± 0.021	8.650	–1.430 ± 0.010	–1.132 ± 0.011	2.337 ± 0.008	0.863
510	708- 52175- 147	J025540.01-002240.0	1.187 ± 0.081	8.189 ± 0.061	8.163	–1.434 ± 0.035	–0.871 ± 0.017	2.216 ± 0.034	0.713
511	708- 52175- 155	J025436.22+000339.9	1.443 ± 0.040	7.890 ± 0.024	7.983	–1.691 ± 0.016	–1.059 ± 0.009	2.483 ± 0.015	0.805
512	708- 52175- 172	J025324.24-000716.6	1.276 ± 0.063	8.100 ± 0.044	8.211	–1.424 ± 0.033	–0.901 ± 0.013	2.245 ± 0.031	0.763
513	708- 52175- 299	J025020.86-005828.9	1.338 ± 0.087	7.962 ± 0.048	8.493	–1.052 ± 0.009	–0.664 ± 0.009	1.658 ± 0.007	0.599
514	708- 52175- 579	J025536.26+005609.6	1.235 ± 0.071	8.069 ± 0.047	8.106	–1.249 ± 0.010	–0.729 ± 0.008	1.924 ± 0.008	0.671
515	710- 52203- 611	J031314.21+004726.5	1.506 ± 0.126	7.903 ± 0.059	8.163	–1.270 ± 0.063	–0.751 ± 0.022	1.962 ± 0.059	0.621
516	712- 52179- 108	J032708.26-002551.9	1.212 ± 0.071	8.212 ± 0.055	8.186	–1.421 ± 0.020	–0.878 ± 0.052	2.292 ± 0.017	0.762
517	712- 52199- 115	J032708.26-002551.9	1.209 ± 0.057	8.205 ± 0.046	8.235	–1.392 ± 0.018	–0.833 ± 0.051	2.267 ± 0.016	0.779
518	713- 52178- 213	J033211.81-004416.0	1.785 ± 0.195	7.588 ± 0.064	8.686	–0.844 ± 0.008	–0.645 ± 0.011	1.275 ± 0.004	0.480
519	713- 52178- 496	J033319.20+001731.2	1.248 ± 0.036	8.136 ± 0.028	8.403	–1.264 ± 0.026	–0.942 ± 0.011	2.118 ± 0.024	0.790
520	714- 52201- 91	J034254.29-005520.2	1.046 ± 0.060	8.332 ± 0.060	8.169	–1.378 ± 0.031	–0.903 ± 0.014	2.179 ± 0.030	0.770
521	802- 52289- 423	J030135.57+011420.0	1.340 ± 0.037	8.059 ± 0.034	7.907	–1.884 ± 0.054	–1.481 ± 0.031	2.857 ± 0.051	0.940
522	804- 52286- 85	J031918.24-005859.1	1.093 ± 0.067	8.298 ± 0.062	8.186	–1.446 ± 0.020	–0.969 ± 0.012	2.276 ± 0.018	0.773
523	805- 52586- 144	J032708.26-002551.9	1.243 ± 0.038	8.174 ± 0.030	8.147	–1.364 ± 0.013	–0.839 ± 0.049	2.257 ± 0.011	0.797
524	805- 52586- 482	J032713.08+003112.3	1.108 ± 0.041	8.249 ± 0.037	8.201	–1.314 ± 0.012	–0.856 ± 0.007	2.115 ± 0.010	0.776
525	805- 52586- 550	J032750.16+010135.0	1.006 ± 0.045	8.355 ± 0.041	8.471	–1.106 ± 0.006	–0.695 ± 0.005	1.747 ± 0.004	0.614
526	805- 52586- 605	J033128.46+003737.2	1.289 ± 0.087	8.036 ± 0.058	8.056	–1.473 ± 0.020	–0.832 ± 0.011	2.181 ± 0.016	0.682
527	806- 52592- 587	J033653.64+005657.4	1.285 ± 0.077	8.055 ± 0.047	8.100	–1.456 ± 0.022	–0.823 ± 0.018	2.151 ± 0.019	0.649
528	811- 52669- 415	J030903.89+003846.6	1.512 ± 0.049	7.932 ± 0.034	8.071	–1.844 ± 0.037	–1.267 ± 0.022	2.801 ± 0.034	0.903
529	960- 52466- 61	J134225.32+582432.7	1.158 ± 0.034	8.194 ± 0.032	8.486	–1.393 ± 0.010	–0.999 ± 0.011	2.232 ± 0.008	0.823
530	972- 52428- 368	J165844.50+351923.1	1.125 ± 0.036	8.216 ± 0.031	8.317	–1.215 ± 0.008	–0.792 ± 0.007	1.957 ± 0.006	0.715
531	978- 52431- 415	J171400.93+313023.4	1.024 ± 0.048	8.335 ± 0.046	8.608	–1.035 ± 0.008	–0.842 ± 0.014	1.749 ± 0.006	0.696